# A Computational Study of Graphene and Phosphorene for DNA Base Detection

A Thesis
by
MATTHEW B. HENRY

Submitted to the Jackson College of Graduate Studies of the
University of Central Oklahoma
in partial fulfillment of the requirements for the degree of
MASTER OF SCIENCE

Chair of Committee:
Benjamin O. Tayo

Committee Members:
Weldon J. Wilson
James Creecy

Chair of Department:
Charles Hughes

December 2020

Major Subject: Engineering Physics-Physics

# A Computational Study of Graphene and Phosphorene for DNA Base Detection

By Matthew Henry

12/04/2020

Jackson College of Graduate Studies at the University of Central Oklahoma

A THESIS APPROVED FOR

Matthew Henry

By

Committee Chairperson

Benjamin Tayo

Committee Member

Weldon Wilson

Committee Member

James P. Creecy

# Abstract

Research into methods of deoxyribonucleic acid (DNA) sequencing has been improving with the goal of providing fast and cheap sequencing of longer strands as accurately as possible. One possible way of improving the process is utilizing a solid-state device. In fact, it has been shown in previous studies that two-dimensional (2D) materials such as graphene, molybdenum disulfide, and hexagonal boron nitride can be used to detect individual DNA bases [2, 3]. Graphene's success for nanopore DNA sequencing has shown that it is possible to explore other potential single- and few-atom thick layers of 2D elemental materials beyond graphene, and also that these materials can exhibit fascinating and technologically useful properties for DNA base detection that are superior to those of graphene. One material of interest is monolayer black phosphorus, or phosphorene. Phosphorene shares many of the remarkable properties of graphene including high carrier mobility [30] and tunable optical properties [32]. The advantage of phosphorene is its direct band gap [31] that is also dependent on thickness, making phosphorene ideal for electronic and optoelectronic applications [33]. It is therefore extremely important to perform exploratory studies to determine phosphorene's ability to detect individual DNA bases as this material is currently being sought after by many experimental groups as a promising material for designing nano-bioelectronic devices for high-speed DNA sequencing. In this thesis, using density functional theory calculations, we find that single-layer phosphorene is an extraordinary material for DNA sequencing using two advanced detection modalities (i.e., nanopore and nanoribbon). We observe that binding energies of DNA bases using nanopores and nanoribbons of phosphorene are smaller compared to graphene devices. This shows that minimal sticking of DNA bases to phosphorene's surface is expected for phosphorene devices. Furthermore, both nanopore and nanoribbon devices from phosphorene show a characteristic change in the density of states for each base. The band gap of phosphorene is significantly changed compared to other nanomaterials (e.g., $MoS_2$, graphene, silicene, h-BN, and silicon nanowire) due to physisorption of bases on the nanoribbon surface. We also observe that the nanoribbon device performs better than the nanopore devices. Our findings confirm our hypothesis that phosphorene is a promising material for DNA base detection using advanced detection principles such as transverse tunneling current measurements. These results will provide valuable insights for other researchers in this field. Ideas for future research include examining this system using a periodic calculation; simulating a real device and calculating the current spectrum; and expanding the research to include other single-layer materials such as transition-metal dichalcogenides and Van der-Waals heterostructures.

# Acknowledgments

I would like to thank Dr. Benjamin O. Tayo for his advisement and patience throughout the duration of this research. I would also like to thank the University of Central Oklahoma, the High Performance Computing Center (Dr. Lemley and Sam Kelting), and the Department of Engineering and Physics for providing resources such as the Buddy Supercomputer, financial assistance to present this research at multiple conferences, and the conference room we were able to hold socially distanced meetings in. I am very grateful to my committee members Dr. Benjamin O. Tayo, Dr. Weldon Wilson, and Dr. James Creecy for their gracious support, flexibility, and patience in this challenging year. Finally, I would lastly like to recognize my family for their patience and thoughtfulness throughout the completion of this report.

# Table of Contents

# List of Figures

# List of Abbreviations

DFT – Density Functional Theory

DNA – Deoxyribonucleic Acid

2D – Two-dimension

3D – Three-dimension

DOS – Density of States

GNR – Graphene Nanoribbon

GNP – Graphene Nanopore

PNR – Phosphorene Nanoribbon

PNP – Phosphorene Nanopore

HOMO – Highest Occupied Molecular Orbital

LUMO – Lowest Unoccupied Molecular Orbital

SCF – Self Consistent Field

SE – Schrodinger Equation

HPC – High Performance Computing

SLURM – Simple Linux Utility for Resource Management

CPU – Central Processing Unit

GPU – Graphics Processing Unit

BP – Black Phosphorus

hBN – hexagonal Boron Nitride

$MoS_2$ – Molybdenum disulfide

GAMESS – General Atomic and Molecular Electronic Structure System

XYZ File – file for storing x, y, and z coordinates of atoms in a molecular system

NERSC – National Energy Research Supercomputing Center

B3LYP – Becke, 3-parameter, Lee-Yang-Parr exchange-correlation functional

6-31G(d,p) – Gaussian Basis Set with Polarization Functions

# Chapter 1. Introduction

Research in two-dimensional (2D) material science has made great strides over the past decades. Since the discovery of graphene, the search for other 2D materials and their various uses has increased dramatically. Multiple studies have suggested that 2D systems can be used for biosensing methods, including DNA base detection [1-3].

Research into methods of deoxyribonucleic acid (DNA) sequencing has been improving with the goal of providing fast and cheap sequencing of longer strands as accurately as possible. Techniques such as the Sanger method [4], labeling and amplification sequencing [5], and biological nanopore sequencing [2] are just a few examples of popular methods in the field. Biological nanopore sequencing is a promising technique with an iteration introduced by the company Oxford Nanopore, in which a device records changes in the ionic current due to the presence of a base in the pore [2, 6]. Newly proposed methods involve replacing the biological nanopore with a solid-state device [1]. These solid-state devices can provide rapid results at lower costs, all while enhancing control of the system [10].

In fact, it has been shown in previous studies that 2D materials such as graphene, molybdenum disulfide, and hexagonal boron nitride can be used to detect single DNA bases by probing ionic current across a nanopore [2, 3]. Despite the many successes, there continue to be challenges for new researchers. For example, it has been shown that when probing ionic current, DNA passing through the nanopore travels faster than the time resolution of the measurement [7, 8]. To alleviate issues with translocation speed, research in materials beyond graphene and systems other than nanopore systems, such as nanoribbons for physisorption, have been proposed [9]. Adsorption (or physisorption) of DNA bases to the material surface has also been explored in previous studies [3]. However, despite the large number of 2D materials, most research efforts have focused on a small number of candidates such as graphene, $MoS_2$, and hexagonal boron nitride. There is need to explore other 2D materials.

This project looks to further explore these systems and new materials by studying the quantum mechanical properties of each using Density Functional Theory (DFT) rather than the classical ionic current measurements. Computational studies using DFT have been used to gain

understanding of the interactions between DNA bases and 2D materials [3]. By viewing the problem using the methods of DFT, quantum properties such as changes in the electronic structure, band gap, and binding energy can be exposed and studied. DFT calculations will be performed using Gaussian and GAMESS software packages, running on the University of Central Oklahoma 'Buddy' Super-Computer, as well as National Energy Research Scientific Computing Center (NERSC). Each atomic system will be built using Jmol, Maestro, and/or Vesta software. Input files are prepared using the Avogadro input generator.

Using the methods stated here, multiple different materials and systems can be tested for their practicality in acting as a DNA base detection device. In this paper, a computational study using DFT is performed for two materials: graphene and phosphorene, in which a nanopore and a nanoribbon are designed to determine the effectiveness in resolving DNA bases. **Figure 1** below presents the device concepts being explored.

To evaluate the potential of phosphorene for DNA bases detection, we shall compute three evaluation metrics, namely, binding energy, density of states, and energy band gap. We will compare the performance of phosphorene with graphene. In a real device, the tunneling current signal is computed numerically from the integrated density of states (DOS) as in [2], suggesting that a modulation in the density of states plot is proportional to modulations in the current:

$$\mathrm{I}(\mathrm{E}, \mathrm{V_b}) = \frac{\mathrm{e}}{\pi\hbar}\int_0^{\mathrm{E}} \mathrm{DOS}(\mathrm{E} - \mathrm{E}')\mathrm{dE}' \qquad \textbf{(1)}$$

This thesis is organized as follows. In Chapter 2, we present an overview of DFT. In Chapter 3, we computed the electronic structure of DNA bases using DFT. In Chapter 4, we studied the interaction of graphene nanomaterials with DNA bases. In Chapter 5, we studied the interaction of phosphorene nanomaterials with DNA bases. In Chapter 6, we present a thesis summary and conclusion.

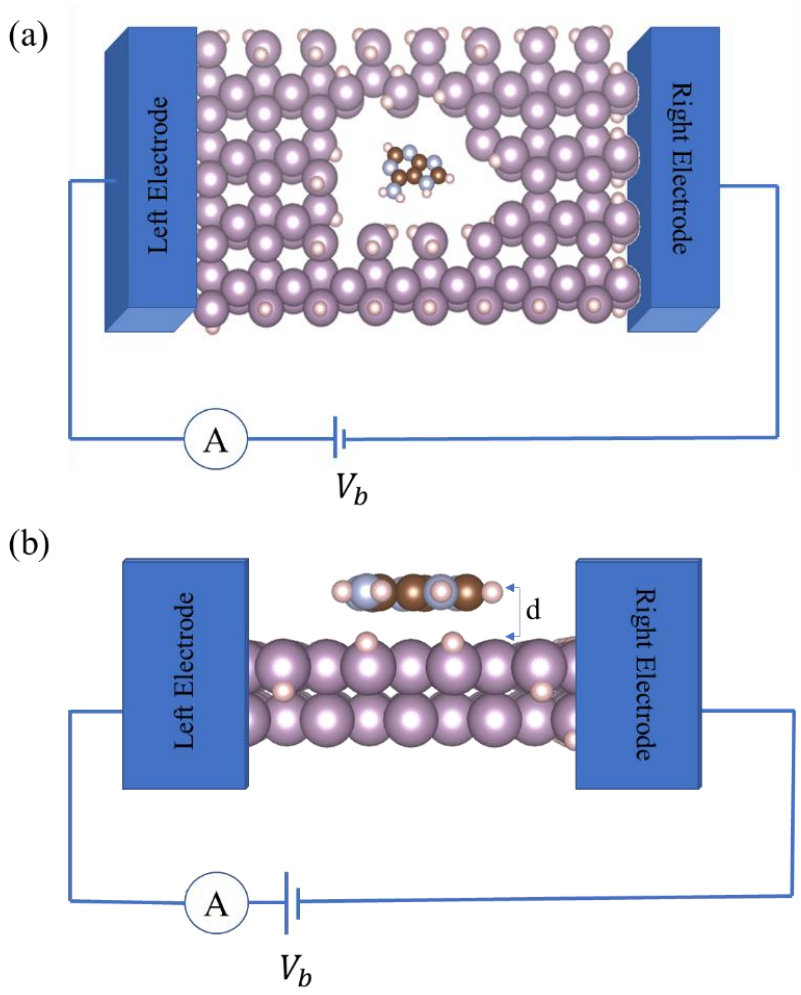


*Figure 1: Concept image for 2D material devices (a) nanopore and (b) physisorption.*

# Chapter 2. Density Functional Theory for Predicting Materials Properties

As research into complex molecules and materials increases, it is becoming more common to perform computational studies to reveal their nature. In the instance of materials, it is extremely helpful to understand the electronic structure to uncover certain properties. To determine the electronic structure requires a serious dose of quantum theory and is not feasibly solved by hand for many-atom systems. Density functional theory (DFT) is a technique used to solve an otherwise very difficult quantum mechanical problem [44]. Hohenburg and Kohn proposed that the density of a system can be used to determine the ground state properties [45]. This is profound in that if you can find the electron density, you can find the total ground-state energy. Although there are multiple software packages that make use of DFT, Gaussian is the focus of our study.

The Gaussian software can act as a "black-box", but it can be helpful to understand the physics behind the calculation. The DFT calculation is basically two main fundamentals: a Self-Consistent Field (SCF) approximation to solve the electron density and the Schrödinger Equation (SE), and a Geometry Optimization that finds the equilibrium of the system. A flowchart outlining the general process behind the DFT study is outlined in **Figure 2** below.

In the SCF portion of the calculation, the initial geometry is used to calculate the total energy as a function of the fixed nuclei. First, an initial guess for the electron density is made. That guess is used to solve the effective potential. The effective potential is used to solve the SE to get an approximate wave function. The wave function is used to calculate a new guess for the electron density. If the density convergence criteria are not met, the process repeats using the new guess for the electron density as the initial guess. If the density convergence criteria are achieved, then the total energy is calculated. Once the SCF cycle is complete, the total energy is sent on to the geometry optimization.

For the geometry optimization, the interatomic forces must be at equilibrium. The gradient of the total energy from the SCF calculation is taken to find the position vector of the nuclei that give a null force. If the force is zero, the geometry optimization is complete. If the force does not equal zero, then the nuclear coordinate $\vec{R}$ is altered and sent back to the SCF initial guess and the process

repeats. Once the force is converged, the final geometry is computed, and the electronic information is saved.

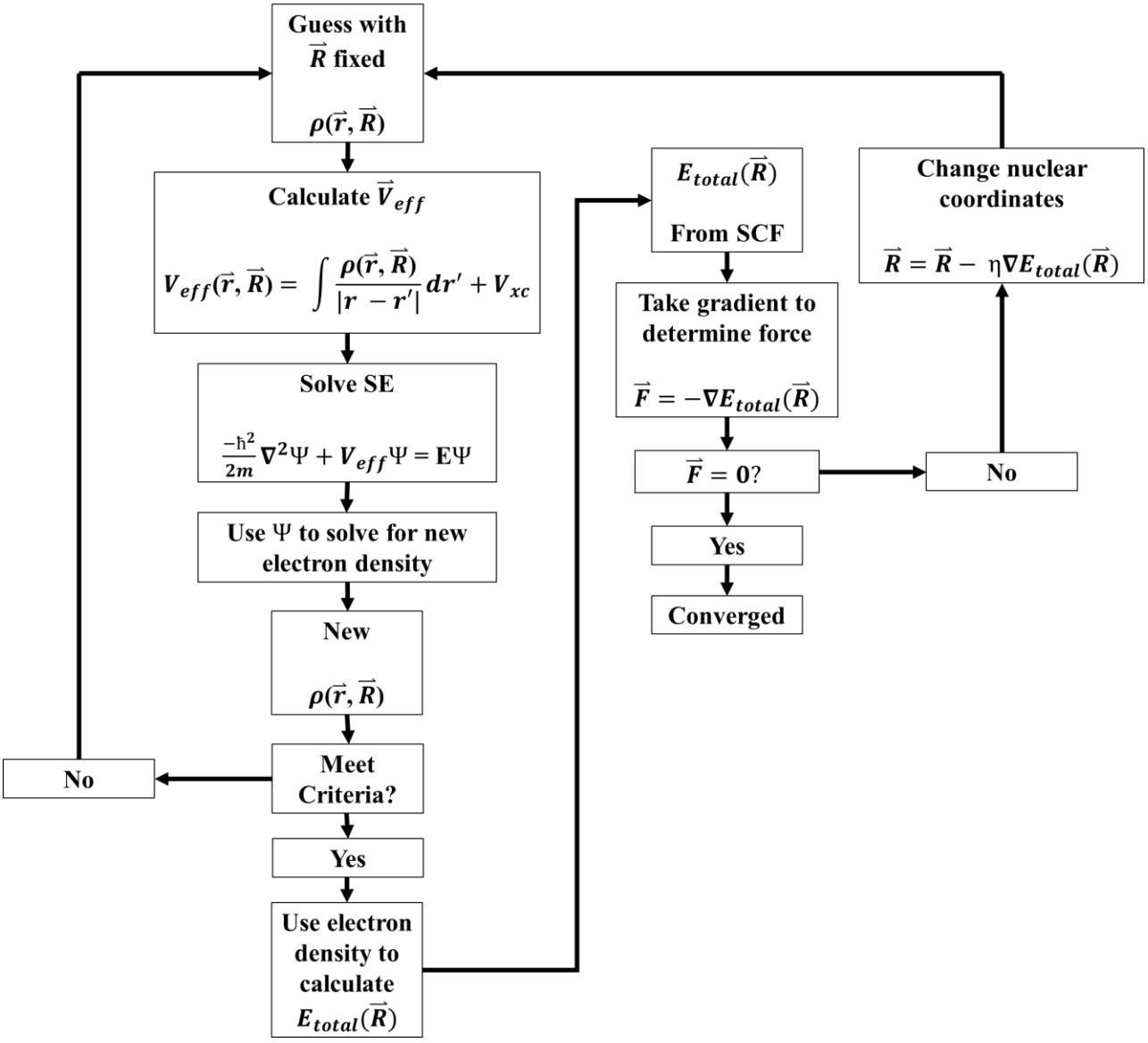


*Figure 2: Fundamentals of DFT flowchart for molecular geometry optimization and electronic structure determination.*

The result of the calculation is the final total energy and the final optimized structure. These results are used to reveal the electronic structure of the system. Because Gaussian can provide the necessary details using a finite system approximation, it is used for calculations on graphene and phosphorene in this study.

### 2.1 Brief Note on Basis Sets

The user cannot simply load the structure into Gaussian and start a calculation. There are several important parameters that must be chosen to run a successful job. The key parameters chosen in Gaussian are the method and basis set. For our calculations we chose B3LYP 6-31G(d,p). B3LYP, Becke, 3-parameter, Lee–Yang–Parr, is chosen as an alternative to the Hartree-Fock method for its known accuracy [46]. 6-31G represents three contracted Gaussian functions to model the core, three contracted Gaussian functions to model the valence, and an additional primitive Gaussian to model the valence [47]. The 'd' adds polarization functions to atoms with more than 2 protons and 'p' adds polarization functions to hydrogen atoms. The added polarization functions improve the total energy calculation [47]. The key to choosing an appropriate basis set is finding the balance between a high-accuracy approximation and the computational cost of the calculation.

### 2.2 Information on Geometry Calculation

To run a geometry optimization 'Opt' is added to the input line. As the number of atoms in the system increases, the DFT calculation takes more time to complete or could even fail to converge. For difficult to converge systems, SCF = QC or SCF = XQC can be added in the input file. The default SCF in Gaussian is a linear style step. SCF = QC adds a quadratic convergence step and SCF = XQC adds an extra SCF = QC step if the first order SCF has not converged [49].

### 2.3 High Performance Computing (HPC) with Buddy

Calculations were submitted to Buddy super-computer at the University of Oklahoma. Buddy received initial funding from the National Science Foundation [48]. Available resources include access to multiple software packages, remote access, nearly 40 nodes for running calculations, and a strong IT support team. GAMESS and Gaussian are installed for computational chemistry and physics calculations. A resource restriction on the number of nodes available to each user is imposed to ensure low queue times, and fairness among the various research groups taking advantage of the super-computer. For sample batch script files see **Appendix B**. A preliminary study of how to select the number of nodes to use in Buddy calculations was performed with a Gaussian calculation on the DNA base adenine. The results of that study are plotted in **Figure 3** below. As the number of nodes increases, the amount of the time the calculation takes is reduced.

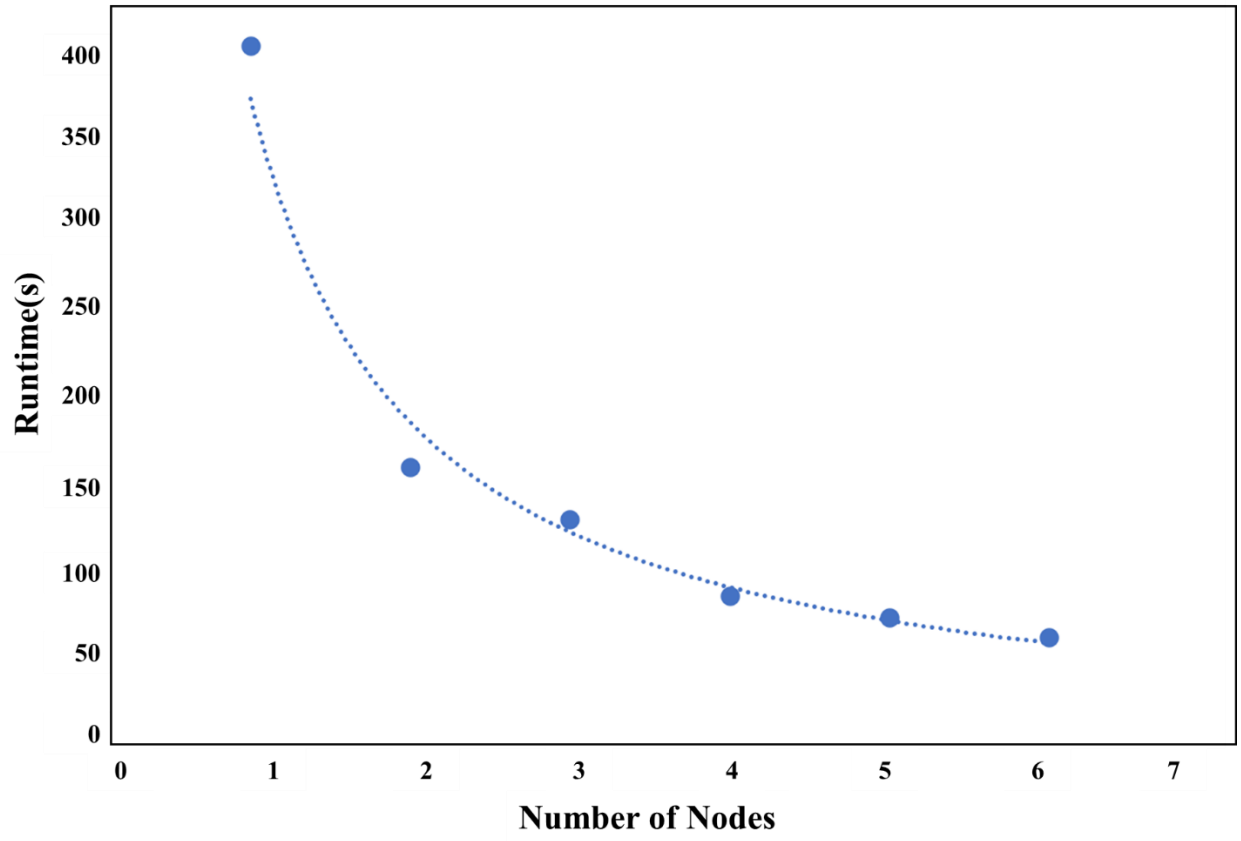


*Figure 3: Runtime vs. Number of nodes for the DNA base adenine.*

# Chapter 3. DFT Studies of Individual DNA Bases

Research into methods of DNA sequencing has been improving with the goal of providing fast and cheap sequencing of longer strands as accurately as possible. Although current methods briefly discussed in the introduction are effective, the strive for solid-state device sequencing is ever promising. It is possible to perform first-principle calculations on these devices to reveal information about their usability as DNA sequencing devices. The goal of this research is to perform DFT studies on 4 systems: Graphene Nanopore, Graphene Nanoribbon, Phosphorene Nanopore, and Phosphorene Nanoribbon. For each device, respective DNA bases are introduced to the system and DFT calculations are performed. As an exercise of our available software, we have performed DFT studies on each of the DNA bases.

### 3.1 Building the Structure of DNA Bases

Although ssDNA presents with bases attached to a phosphate helix, it is reasonable to ignore the repeating phosphate group to reduce the system being studied. The distance between bases in ssDNA is 0.63 nm on average [40]. This small distance is the exact reason 2D materials would be favorable in single base resolution devices. The 2D material graphene is a single atom thick and phosphorene is only slightly thicker. The thickness of each material allows for interaction with a single base at a time. Each DNA base structure is loaded from the software Jmol [25]. The structures of Adenine, Cytosine, Guanine, and Thymine used for creating the input files are seen in **Figure 4** below.

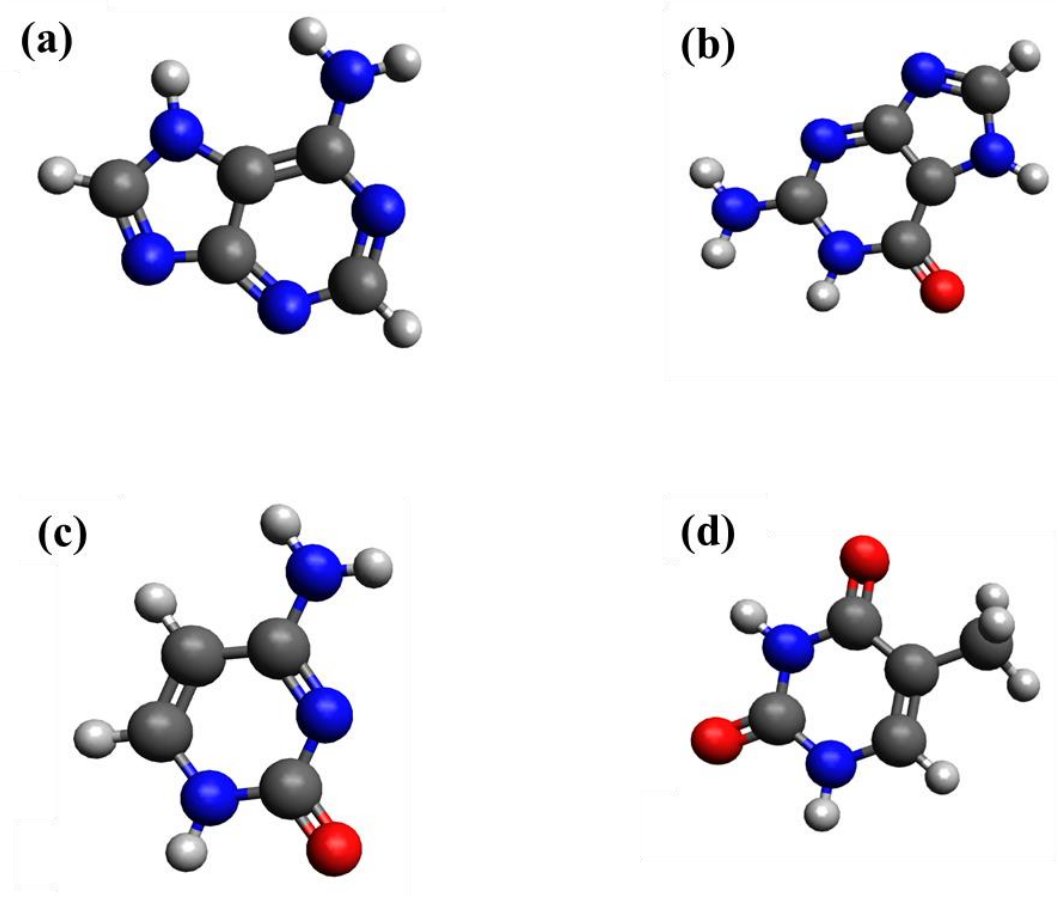


*Figure 4: Jmol ball and stick structure of (a) Adenine, (b) Guanine, (c) Cytosine, and (d) Thymine. Blue atoms are nitrogen, gray atoms are carbon, red atoms are oxygen, and white atoms are hydrogen.*

### 3.2 Input Files for DNA Bases

The DFT study for DNA bases was performed using two software packages: GAMESS [41], and Gaussian [27]. Input files for Gaussian can be created using the molecular editor Avogadro. Using the Avogadro Gaussian input generator, an editable input file is created. A sample Gaussian input file for Adenine is seen in **Figure 5** below. For a complete input file example, see **Appendix A**.

```
#n B3LYP/6-31G(d,p) Opt

 Title

0 1
N          -1.97190       -0.36881        0.00000
C          -1.48450       -1.59610        0.00000
N          -0.19340       -1.84410        0.00010
C           0.69130       -0.84200       -0.00020
N           2.03570       -0.77000        0.00030
C           2.41080        0.47890        0.00020
N           1.32860        1.28940       -0.00030
C           0.21300        0.47880       -0.00060
C          -1.16680        0.69050       -0.00020
N          -1.68630        1.97500        0.00040
H          -2.17300       -2.42820        0.00020
H           3.43660        0.81670        0.00080
H           1.33560        2.25940       -0.00020
H          -1.08930        2.73960        0.00060
H          -2.64690        2.10970        0.00060

```

*Figure 5: Gaussian input file for adenine.*

The input file is of the file type *filename.com* and is saved in the running directory. Note the basis set 6-31G(d.p), the method B3LYP, and the calculation type is a geometry optimization 'Opt'. For geometry optimization calculations, the atoms were relaxed until the force between atoms was less than 0.02 eV/Å. This convergence criterion is the standard threshold in Gaussian 16 software and is comparable with what has been used in other computational studies [9]. For the rest of our calculations, the force convergence criterion will be set at 0.02 eV/Å.

The GAMESS software requires a different input file and can also be generated using Avogadro. The GAMESS calculation was submitted using the nanoHUB MIT Atomic Modeling Toolkit, which generates its own input file [41].

### 3.3 Running Calculations for DNA Bases

The Gaussian calculation was submitted locally on the University of Central Oklahoma super-computer 'Buddy'. Buddy requires Simple Linux Utility for Resource Management (SLURM) formatted batch script files to submit jobs. A sample batch script file is seen below in **Figure 6**. The file is saved as file type *filename.sh* in the running directory. See a full sample batch script file in **Appendix B.**

```
#!/bin/bash
#SBATCH --job-name=g16
#SBATCH --nodes=2
#SBATCH --cpus-per-task=20
#SBATCH --output=g16-%j.out

### Of the batch options, it is only recommnded to change "--job-name", "--nodes", and
### "--output". Any other modifications may result in an error.

### It is only recommneded to change the input file in the Gaussian command. If needed
### more g16 options can be added.

#Load Gaussian module
module load Gaussian/g16

#Gaussian scratch directory.
export GAUSS_SCRDIR=/home/$USER/.gaustmp/$SLURM_JOBID
mkdir -p $GAUSS_SCRDIR

#Stop OpenMP from interfering with Gaussian's thread mechanism.
export OMP_NUM_THREADS=1

#Prepare node list for Linda
for n in `scontrol show hostname | sort -u`; do
  echo ${n}
done | paste -s -d, > snodes.$SLURM_JOBID

#Run Gaussian. It is recommended to only change the input file here. If needed you can
#raise the memory up to 60GB, but doing so may result in an error.
g16 -m=40gb -p=${SLURM_CPUS_PER_TASK} -w=`cat snodes.$SLURM_JOBID` adenine.com

#Clean up nodes list
rm snodes.$SLURM_JOBID
```

*Figure 6: Sample SLURM batch script file.*

The GAMESS calculation was submitted using the nanoHUB MIT Atomic Modeling Toolkit. The toolkit requires the user to input the calculation parameters and the XYZ file of the structure. The toolkit runs the calculation and then generates output files of the optimized structure.

### 3.4 GAMESS Results

The GAMESS output file provides final optimized geometry of the structure. An example of the optimized structure is seen in **Figure 7**. The optimized structure can be opened in the software MACMOLPLT [42]. This software allows the user to visualize the geometry optimization in steps.

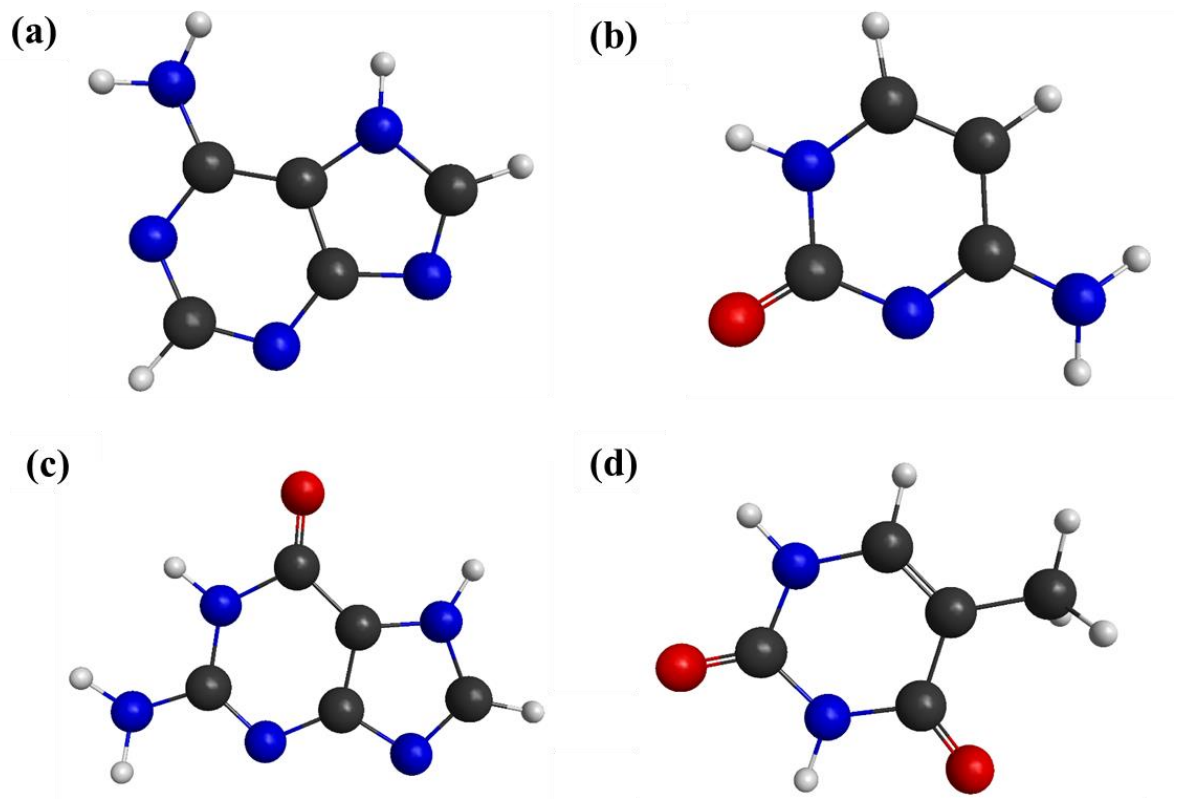


*Figure 7: Optimized geometries for (a) adenine, (b) cytosine, (c) guanine, and (d) thymine using DFT.*

Once the GAMESS calculation is complete, the user can choose to download the output files. The MIT Toolkit produces additional files that outline information of interest. **Figure 8** shows the GAMESS generated energy gap file for the adenine calculation. Note the difference in lowest unoccupied molecular orbital (LUMO) and the highest occupied molecular orbital (HOMO) levels make up the energy gap.

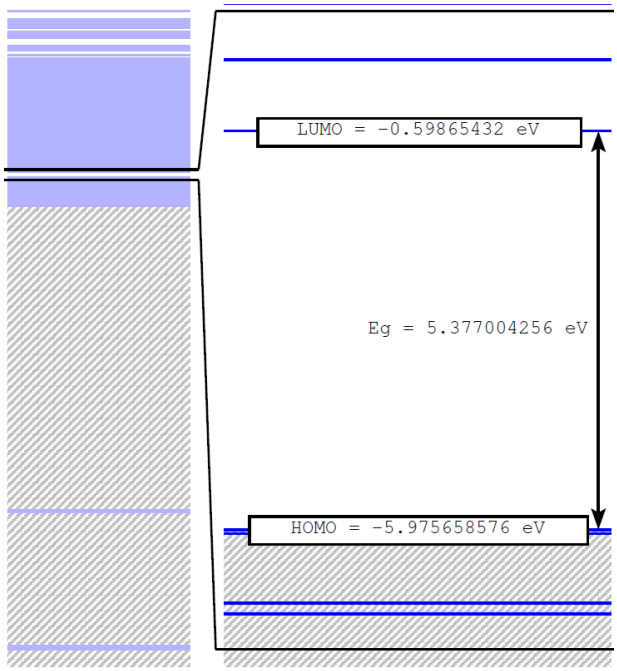


*Figure 8: Energy Gap for Adenine from nanoHUB MIT Atomic Modeling Toolkit.*

The energy gap for each base is recorded in **Table 1** below.

*Table 1: Energy Gap for each DNA base from GAMESS calculation.*

| **Base** | **LUMO (eV)** | **HOMO (eV)** | **$E_{gap}$ (eV)** |
|---|---|---|---|
| **Guanine** | -0.310 | -5.374 | 5.064 |
| **Adenine** | -0.598 | -5.975 | 5.377 |
| **Cytosine** | -0.895 | -5.861 | 4.966 |
| **Thymine** | -0.987 | -6.375 | 5.387 |

### 3.5 Gaussian Results

Once the Gaussian calculation is completed, an output file of the file type *filename*.log is saved to the running directory. Key information to extract from the output file includes the final energy, the HOMO and LUMO levels, and the final geometry. Excerpts from an output file are seen in **Figures 9 - 12** below. Note the confirmation of convergence, the normal termination message, the energy gap, and the final total energy.

```
  D32       -3.14159   0.00000   0.00001   0.00005   0.00006  -3.14153
        Item               Value     Threshold  Converged?
Maximum Force            0.000281     0.000450     YES
RMS     Force            0.000067     0.000300     YES
Maximum Displacement     0.001528     0.001800     YES
RMS     Displacement     0.000320     0.001200     YES
Predicted change in Energy=-5.475167D-07
Optimization completed.
   -- Stationary point found.
```

*Figure 9: Confirmation of convergence from excerpt of a Gaussian output file.*

```
Job cpu time:       0 days  0 hours  0 minutes  9.3 seconds.
Elapsed time:       0 days  0 hours  3 minutes 13.8 seconds.
File lengths (MBytes):  RWF=     33 Int=      0 D2E=      0 Chk=      4 Scr=      2
Normal termination of Gaussian 16 at Tue May 26 17:13:21 2020.
```

*Figure 10: Normal termination message from excerpt of Gaussian output file.*

```
Alpha  occ. eigenvalues --  -14.40963 -14.36787 -14.32289 -14.32066 -14.31305
Alpha  occ. eigenvalues --  -10.28225 -10.26656 -10.24097 -10.23845 -10.23197
Alpha  occ. eigenvalues --   -1.03332  -0.97706  -0.93456  -0.88766  -0.85089
Alpha  occ. eigenvalues --   -0.76944  -0.66590  -0.64868  -0.62617  -0.58931
Alpha  occ. eigenvalues --   -0.54405  -0.52014  -0.50595  -0.46298  -0.45806
Alpha  occ. eigenvalues --   -0.45290  -0.40662  -0.40109  -0.35588  -0.29978
Alpha  occ. eigenvalues --   -0.29416  -0.27598  -0.25901  -0.24373  -0.22419
Alpha virt. eigenvalues --   -0.02321   0.00775   0.03174   0.05101   0.09083
Alpha virt. eigenvalues --    0.12042   0.13325   0.16467   0.17043   0.19357
Alpha virt. eigenvalues --    0.22450   0.24710   0.26833   0.28929   0.32947
Alpha virt. eigenvalues --    0.35900   0.37033   0.38964   0.44690   0.47195
Alpha virt. eigenvalues --    0.50753   0.52611   0.54159   0.55177   0.58088
Alpha virt. eigenvalues --    0.58956   0.60064   0.62198   0.63286   0.63939
Alpha virt. eigenvalues --    0.64525   0.67373   0.68652   0.68910   0.69457
Alpha virt. eigenvalues --    0.73569   0.76488   0.78253   0.78765   0.81522
Alpha virt. eigenvalues --    0.82190   0.82363   0.84119   0.84469   0.84656
```

*Figure 11: Energy Gap from excerpt of Gaussian output file.*

```
Requested convergence on RMS density matrix=1.00D-08 within 128 cycles.
Requested convergence on MAX density matrix=1.00D-06.
Requested convergence on             energy=1.00D-06.
No special actions if energy rises.
SCF Done:  E(RB3LYP) =  -467.317150275     A.U. after    9 cycles
           NFock=  9  Conv=0.50D-08     -V/T= 2.0092
Calling FoFJK, ICntrl=      2127 FMM=F ISym2X=0 I1Cent= 0 IOpClX= 0 NMat=1 NMatS=1 NMatT=0.
***** Axes restored to original set *****
```

*Figure 12: Total Energy from excerpt of Gaussian output file.*

The HOMO level, LUMO level, and energy gap are shown in **Table 2** below.

*Table 2: LUMO level, HOMO level, and Energy gap for each DNA base as calculated in Gaussian.*

| System | LUMO (eV) | HOMO (eV) | $E_{gap}$ (eV) | $E_{total}$ (eV) |
|---|---|---|---|---|
| **Guanine** | -0.514 | -5.599 | 5.085 | -14749.874 |
| **Adenine** | -0.631 | -6.097 | 5.466 | -12703.984 |
| **Cytosine** | -0.782 | -6.139 | 5.356 | -10736.544 |
| **Thymine** | -1.027 | -6.566 | 5.539 | -12346.174 |

### 3.6 Gaussian Density of States

A density of states (DOS) plot can be computed for visualization of molecular energy levels. The finite temperature DOS is given by:

$$DOS\,(E) = \sum_i \frac{\Gamma}{(E-E_i)^2+\Gamma^2} \quad \textbf{(2)}$$

where the summation is over the number of molecular energies $E_i$, and $\Gamma$ represents the linewidth (or energy resolution). The energy resolution is chosen to be 25.9 meV to mimic the thermal energy at room temperature. The density of states plot is created using Wolfram Mathematica. See **Appendix C** for sample Mathematica DOS code. The final energy levels of the optimized structure are extracted from the output file and converted to data file (*.dat file* type). The file is imported into Mathematica and cleaned to create a list of energies $E_i$. These energies are then used in **Equation 1** to compute the DOS.

**Figure 13** below shows the DOS for each DNA base. The dotted line in each figure represents the position of the Fermi energy which is approximated as

$$E_F = \frac{E_{HOMO}+E_{LUMO}}{2} \quad \textbf{(3)}$$

where $E_{HOMO}$ and $E_{LUMO}$ are the HOMO and LUMO energies, respectively.

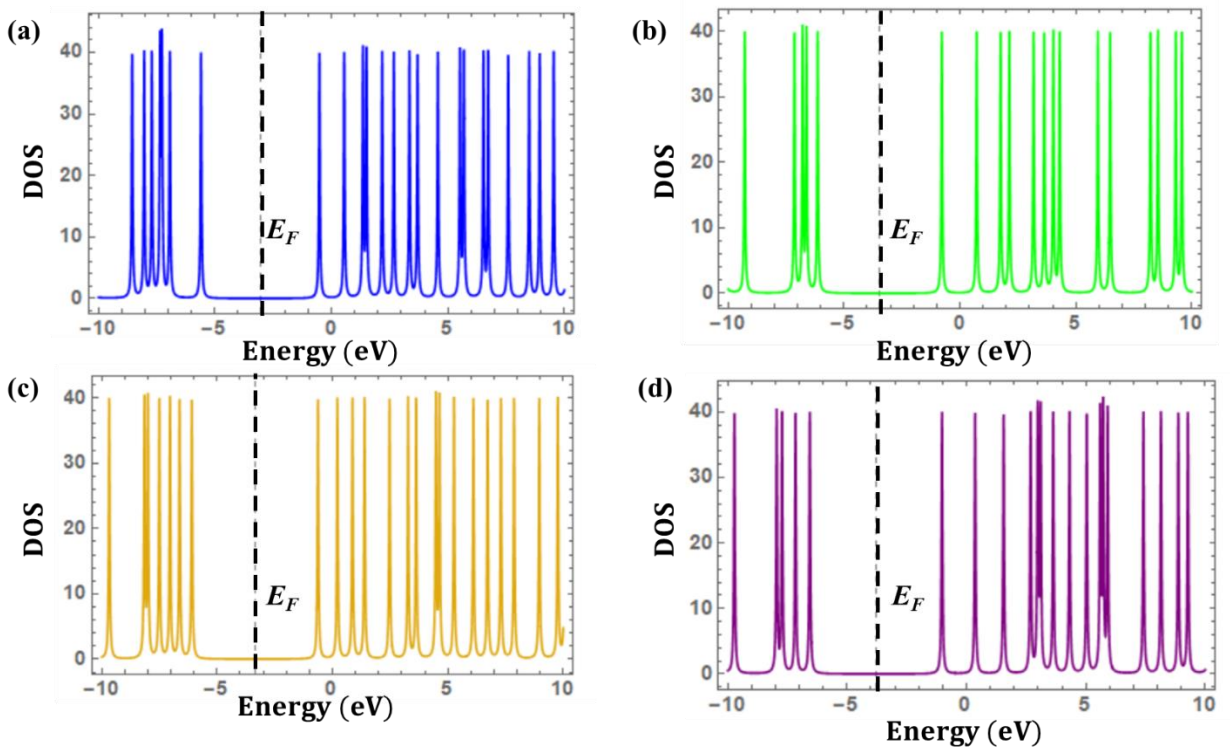


*Figure 13: Density of States plot for (a) Guanine, (b) Cytosine, (c) Adenine, and (d) Thymine.*

It is interesting to note that a similar result was obtained in the publication "Electronic Properties of DNA Base Molecules Adsorbed on a Metallic Surface" [43]. In our studies, the energy gap of each base was computed (using GAMESS and Gaussian codes) and compared with experimental values, as shown in **Table 3**. Our computed results agree nicely with other experimental and theoretical values reported in the literature.

*Table 3: Comparison of Gaussian, GAMESS, and previously obtained values for energy gaps of each base.*

| **Base** | **Gaussian** | **GAMESS** | **Theoretical [43]** | **Experimental [43]** |
|---|---|---|---|---|
| **Guanine** | 5.085 | 5.064 | 5.59 | 4.46 |
| **Adenine** | 5.466 | 5.377 | 5.31 | 4.47 |
| **Cytosine** | 5.356 | 4.966 | 5.21 | 4.31 |
| **Thymine** | 5.539 | 5.387 | 5.41 | 4.64 |

Because Gaussian is used to complete calculations for the remaining systems (graphene nanomaterials + DNA bases; and phosphorene nanomaterials + DNA bases), the final equilibrium geometry and total energy from those calculations will be used throughout the remainder of our calculations to calculate binding energies between DNA bases and 2D nanomaterial systems (nanopores and nanoribbons).

# Chapter 4. Interaction of Graphene Nanomaterials with DNA Bases

Graphene is a 2D material, only one atom thick, constructed entirely of carbon atoms arranged in a hexagonal lattice structure. Graphene is often described as a single layer of 3D graphite, or the unrolled structure of a carbon nanotube, and was the term originally used to describe theoretical 2D carbon materials up until the confirmation of its existence in the mid-2000s [11-13].

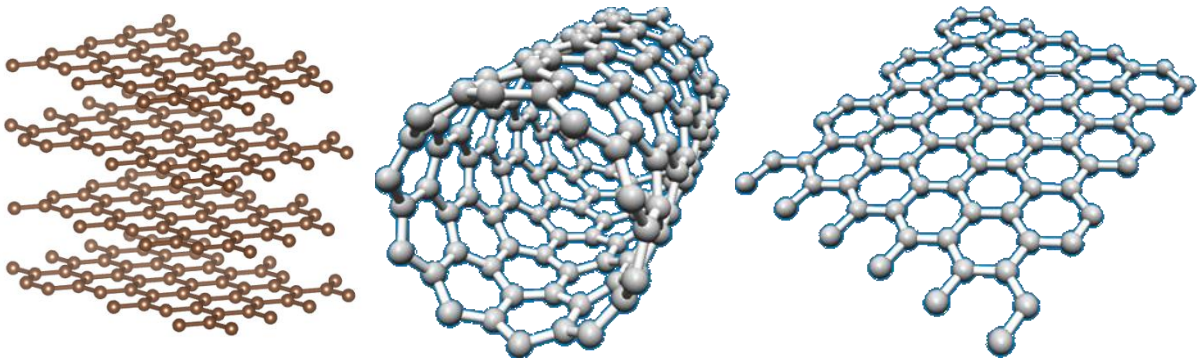

*Figure 14: (left) Graphite structure as visualized in Vesta, (middle) Graphene nanotube as visualized in Nanotube Modeler, and (right) Graphene Nanoribbon as visualized in Nanotube Modeler.*

Graphene is known to display amazing mechanical and electrical properties such as its strength [12], thermal abilities [15], electron transport mobility [16], and the ability to be tuned to suit certain needs [17]. Graphene has multiple means of production and researchers are constantly searching for better ways to mass produce it. Popular production methods include mechanical exfoliation [13] and chemical vapor deposition [19] among others. A brand-new study by Rice University even suggests flash heating garbage to create graphene, a promising technique for large scale mass production [20]. One particularly interesting structure of graphene is the Graphene Nanoribbon (GNR). A GNR is a finite sized structure of graphene that can often be classified by its width and length. The GNR maintains many of the remarkable properties of graphene. The band gap is dependent on the width of the GNR [17] and electron mobility across the surface of the GNR is only obstructed by the edges of the sheet [21]. It has been suggested that 2D materials, such as GNRs, can be used for biosensing applications. In fact multiple methods have been proposed, such as measuring changes in ionic current through a nanopore due to presence of DNA bases [22, 23], modulation in tunneling current across a nanogap, current changes across the plane of a nanopore, and lastly the adsorption of DNA to the surface (physisorption) [2]. The following section outlines results obtained through our own research, performing a DFT study of the graphene nanopore (GNP).

### 4.1 Graphene Nanopore (GNP)

The initial graphene nanoribbon structure was created using the software package Nanotube Modeler [24]. The software provides the ability to set the width and length of the GNR and it is imperative to determine the size. Our study chose the size 7W by 4T which measures to be 1.78 nm by 1.88 nm. 7W indicates 7 hexagons across, and the 4T indicates the height.

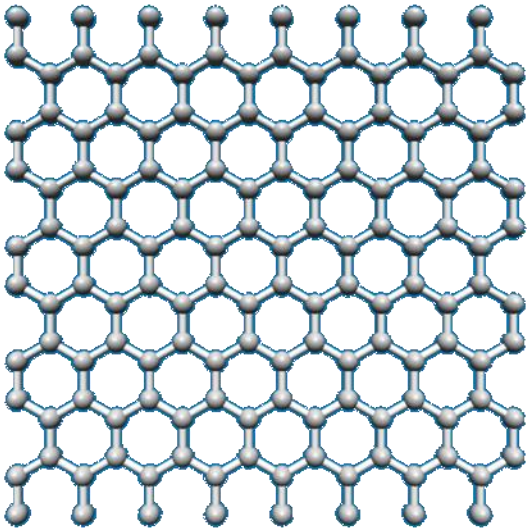

*Figure 15: Initial Graphene structure created in Nanotube Modeler.*

This size was chosen to keep the number of atoms at a minimum while maintaining a large enough structure to contain the nanopore and DNA base. Too large of a system can result in wasted computational space. Once the GNR is created, a XYZ formatted file is saved.

The XYZ file can be opened using the software Maestro [26]. Maestro was selected as the primary atomic modeler due to its ability to merge structures. The XYZ file for each DNA base and the GNR were loaded into the software. DNA bases were each measured to determine the minimum size of the nanopore.

*Table 4: DNA Base maximum width.*

| **DNA Base** | **Maximum Width (nm)** |
|---|---|
| **Guanine** | 0.754 |
| **Adenine** | 0.648 |
| **Cytosine** | 0.560 |
| **Thymine** | 0.590 |

The ‘widest’ DNA base, Guanine at 0.754 nm, was then overlaid onto the GNR structure. Using the ‘delete atom function’, carbon atoms were removed until a pore large enough to contain guanine was constructed. The pore must be large enough in diameter to support all orientations of each DNA base. Our pore diameter measures approximately 1.1 nm, which is in the 1-2 nm range proposed in previous studies [2]. The overlaid guanine was then removed and the XYZ file of the GNP was saved. Hydrogen atoms were added to the edges of the sheet and the pore to neutralize the charge of any dangling bonds. Each DNA base was then placed into the pore, nearest the center as possible, and respective XYZ files were saved. Each DNA base was oriented planar to the GNP surface. Saved structures for calculations include GNP, GNP + Adenine, GNP + Cytosine, GNP + Guanine, and GNP + Thymine. An example structure for GNP and GNP + Adenine are seen in **Figure 16** below.

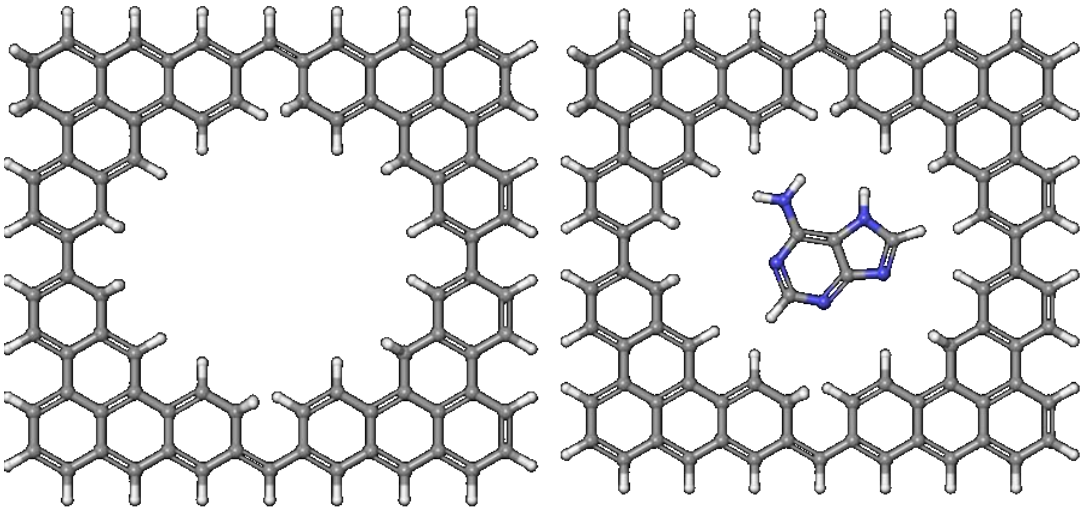

*Figure 16: GNP, and GNP with Adenine.*

### 4.1.1 Creating Graphene Nanopore Input Files

The software package used to run computations is known as Gaussian, we used version 16 [27]. The software requires input files to set computation parameters and settings, as well as load the structure of the system to be tested. Gaussian input files are of the file type *filename*.com. Although it is possible to create these input files from scratch, it is helpful to make use of other software packages to autogenerate a template input file. Our study made use of software known as Avogadro [28]. Avogadro is a molecular editor but also has the ability to load XYZ structures and generate Gaussian formatted input files. A sample input file can be seen in **Figure 17** below.

```
#n B3LYP/6-31G(d,p) Opt SCF=XQC

 Title

0 1
H          7.38370        0.34100        0.00000
C          8.61440        2.13150        0.00000
C          7.38370        1.42100        0.00000
C          8.61440        3.55250        0.00000
C          7.38370        4.26300        0.00000
C          8.61440        6.39450        0.00000
C          7.38370        5.68400        0.00000
C          8.61440        7.81550        0.00000
C          7.38370        8.52600        0.00000
C          8.61440       10.65750        0.00000
C          7.38370        9.94700        0.00000
C          8.61440       12.07850        0.00000
C          7.38370       12.78900        0.00000
C          8.61440       14.92050        0.00000
C          7.38370       14.21000        0.00000
C          8.61440       16.34150        0.00000
C          7.38370       17.05200        0.00000
H          9.84500        0.34100        0.00000
C         11.07560        2.13150        0.00000
C          9.84500        1.42100        0.00000
C         11.07560        3.55250        0.00000
C          9.84500        4.26300        0.00000
C         11.07560        6.39450        0.00000
C          9.84500        5.68400        0.00000
C         11.07560        7.81550        0.00000
C          9.84500        8.52600        0.00000
C         11.07560       10.65750        0.00000
C          9.84500        9.94700        0.00000
C         11.07560       12.07850        0.00000
C          9.84500       12.78900        0.00000
C         11.07560       14.92050        0.00000
C          9.84500       14.21000        0.00000
```

*Figure 17: Sample Gaussian input file excerpt for large system.*

Each Gaussian input file contains information about the computation and the structure's XYZ coordinates. A breakdown of keywords in the above sample input file follows. The basis-set B3LYP/6-31G(d,p) was chosen as the most fitting approximation for our system (see DFT section for details). After the basis-set selection, the type of calculation is set as 'Opt' which is short for 'geometry optimization'. Lastly, it is often useful to place SCF = QC or SCF = XQC in the file to deal with difficult to converge structures. Below the input lines are the XYZ coordinates of the structure. The file is saved to the running directory, the folder in which the job will be submitted, as the file type *filename*.com.

### 4.1.2 Running Graphene Nanopore Calculations

This project utilized the University of Central Oklahoma super-computer 'Buddy' to run Gaussian. To submit jobs on Buddy, one uses SLURM formatted batch scripts. An example of a batch script file can be found below in **Figure 18**.

```
1  #!/bin/bash
2  #SBATCH --job-name=g16
3  #SBATCH --nodes=2
4  #SBATCH --partition=nodes
5  #SBATCH --cpus-per-task=20
6  #SBATCH --output=g16-%j.out
7
8  ### Of the batch options, it is only recommnded to change "--job-name", "--nodes", and
9  ### "--output". Any other modifications may result in an error.
10
11 ### It is only recommneded to change the input file in the Gaussian command. If needed
12 ### more g16 options can be added.
13
14 #Load Gaussian module
15 module load Gaussian/g16
16
17 #Gaussian scratch directory.
18 export GAUSS_SCRDIR=/home/$USER/.gaustmp/$SLURM_JOBID
19 mkdir -p $GAUSS_SCRDIR
20
21 #Stop OpenMP from interfering with Gaussian's thread mechanism.
22 export OMP_NUM_THREADS=1
23
24 #Prepare node list for Linda
25 for n in `scontrol show hostname | sort -u`; do
26   echo ${n}
27 done | paste -s -d, > snodes.$SLURM_JOBID
28
29 #Run Gaussian. It is recommended to only change the input file here. If needed you can
30 #raise the memory up to 60GB, but doing so may result in an error.
31 g16 -m=40gb -p=${SLURM_CPUS_PER_TASK} -w=`cat snodes.$SLURM_JOBID` graphenesheet.com
32
33 #Clean up nodes list
34 rm snodes.$SLURM_JOBID
```

*Figure 18: Sample SLURM batch script file for a large system.*

Line 1 of the batch script file is the universal start of a batch script file in SLURM. Line 3 indicates the number of nodes the computation uses on the super-computer. Line 4 restricts the computation from unnecessarily using GPU (graphics processing unit) resources. Line 5 sets the number of CPU (central processing unit) per task. Line 6 names the output file. Line 12 loads the Gaussian version 16 software. Lines 14 and 15 define the path to the scratch directory where temporary information is stored. Line 24 runs the job and calls the input file. The batch script file, *filename*.sh, is then saved in the running directory. Using the command line, one navigates to the running directory and uses the command *sbatch filename.sh* to submit the job. It is important to note that the batch script file and the input file be saved in the same directory. **Table 5** below outlines the runtime for each system for the GNP portion of the experiment.

*Table 5: Table of runtimes for GNP systems.*

| System | Number of Nodes | Convergence Criteria | Runtime (hours) |
|---|---|---|---|
| **GNP + Guanine** | 4 | STD | 6.1 |
| **GNP + Adenine** | 4 | STD | 10.6 |
| **GNP + Cytosine** | 4 | STD | 16.2 |
| **GNP + Thymine** | 4 | STD | 13.6 |
| **GNP** | 4 | STD | 1.3 |

### 4.1.3 Graphene Nanopore Results

When a job is completed, the output *filename*.log is found in the running directory. The output file contains information on the entire computational process and is considered a completed run with the phrase 'NORMAL TERMINATION OF GAUSSIAN'. For this study the final geometry, the final energy, and the final energy levels were used to determine the results. Results from each output file are further described below.

### 4.1.3 (a) Binding Energy for GNP with DNA Bases

Given the energy of each the 2D sheet, the 2D sheet with pore, and the 2D sheet with pore and DNA, one can calculate the binding energy of the DNA and the GNP:

$$E_{bind} = E_{GNP+base} - (E_{GNP} + E_{base}) \quad \textbf{(4)}$$

where $E_{bind}$ is the binding energy, $E_{\mathrm{GNP}+base}$ is the total energy of the system (DNA base + 2D material), $E_{\mathrm{GNP}}$ is the energy of the 2D material, and $E_{base}$ is the energy of the base. The binding energy is a key parameter that describes the strength of interaction between DNA and the 2D GNP. **Table 6** below lists the binding energy for each system.

*Table 6: Total Energy, Energy Gap, and Binding Energy for GNP systems.*

| **System** | **$E_{tot}$ (eV)** | **$E_{gap}$ (eV)** | **$E_{bind}$ (eV)** |
|---|---|---|---|
| **GNP + Guanine** | $-1.048 \times 10^5$ | 0.228 | -0.888 |
| **GNP + Adenine** | $-1.027 \times 10^5$ | 0.230 | -0.936 |
| **GNP + Cytosine** | $-1.008 \times 10^5$ | 0.230 | -1.063 |
| **GNP + Thymine** | $-1.024 \times 10^5$ | 0.231 | -0.871 |

### 4.1.3 (b) Optimized Geometry for GNP for Different DNA Bases

The optimized geometry for each GNP system is shown in **Figure 19** below along with each binding energy value**.** Binding energies for our GNP calculation follow the order C >A > G > T.

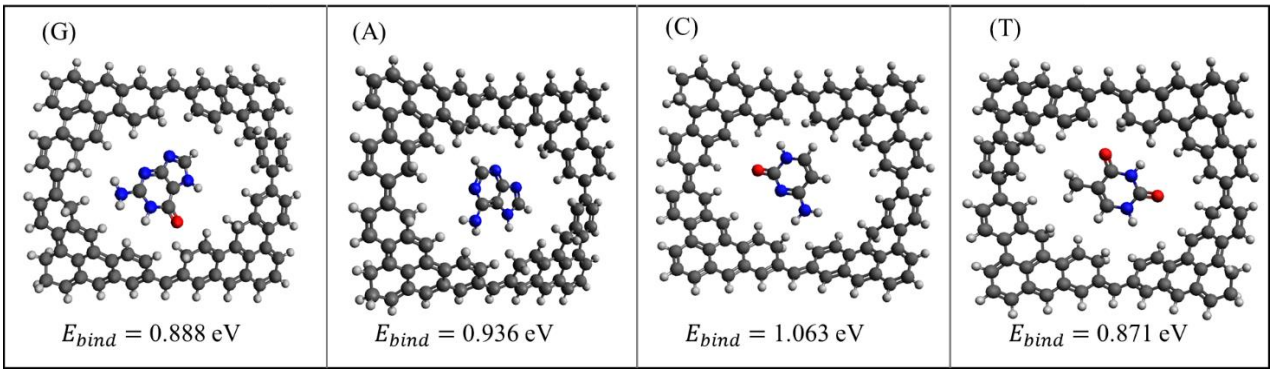


*Figure 19: Optimized structure of GNP systems with binding energy.*

### 4.1.3 (c) Energy Band Gap for GNP with DNA Bases

Noticing the already small energy gap of the 2D material without the pore, it is apparent that electronic detection would be difficult [2]. Also, the energy gap changes very little in the presence of each DNA base, leading to the unlikelihood of the ability to differentiate between signals. **Table 7** outlines the energy gap changes when a DNA base is present in the GNP.

*Table 7: Energy gap for each GNP System.*

| System | LUMO (eV) | HOMO (eV) | $E_{gap}$ (eV) |
|---|---|---|---|
| **GNP** | -3.334 | -3.555 | 0.221 |
| **GNP + Guanine** | -3.213 | -3.441 | 0.228 |
| **GNP + Adenine** | -3.299 | -3.529 | 0.230 |
| **GNP + Cytosine** | -3.276 | -3.506 | 0.230 |
| **GNP + Thymine** | -3.299 | -3.530 | 0.231 |

Finally, we plot the binding energy and band gap as shown in **Figure 20** below.

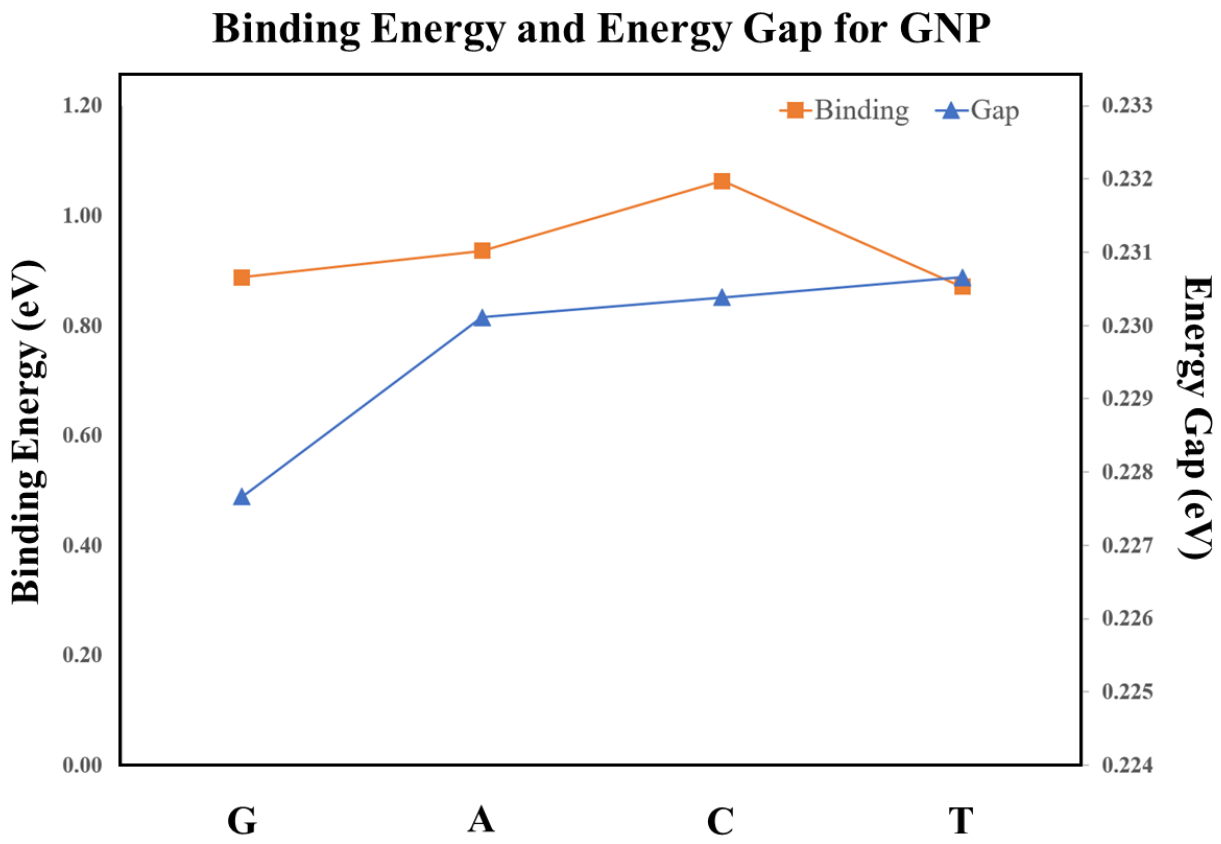


*Figure 20: Binding Energy and Energy Gap vs. Base for GNP systems.*

As seen in the figure, GNP has large binding energies, which shows that the individual bases can easily stick to the surface of the graphene nanopore. Sticking to the surface can cause significant issues with detection. The above figure also shows that there is a minimal change in energy band gap due to the presence of each DNA base. This means that this material would not be ideal for advanced detection using transverse current.

### 4.1.3 (d) Density of States for GNP with DNA Bases

It is also convenient to generate DOS plots to provide visual assistance in determining the usability of GNP as a DNA sensing device. Below are DOS plots for each system, and a combined DOS plot with each system overlaid. The DOS plot makes it is easy to see that there is not a significant difference in each system due to the presence of each base. **Figure 21** below outlines the DOS plot for each system.

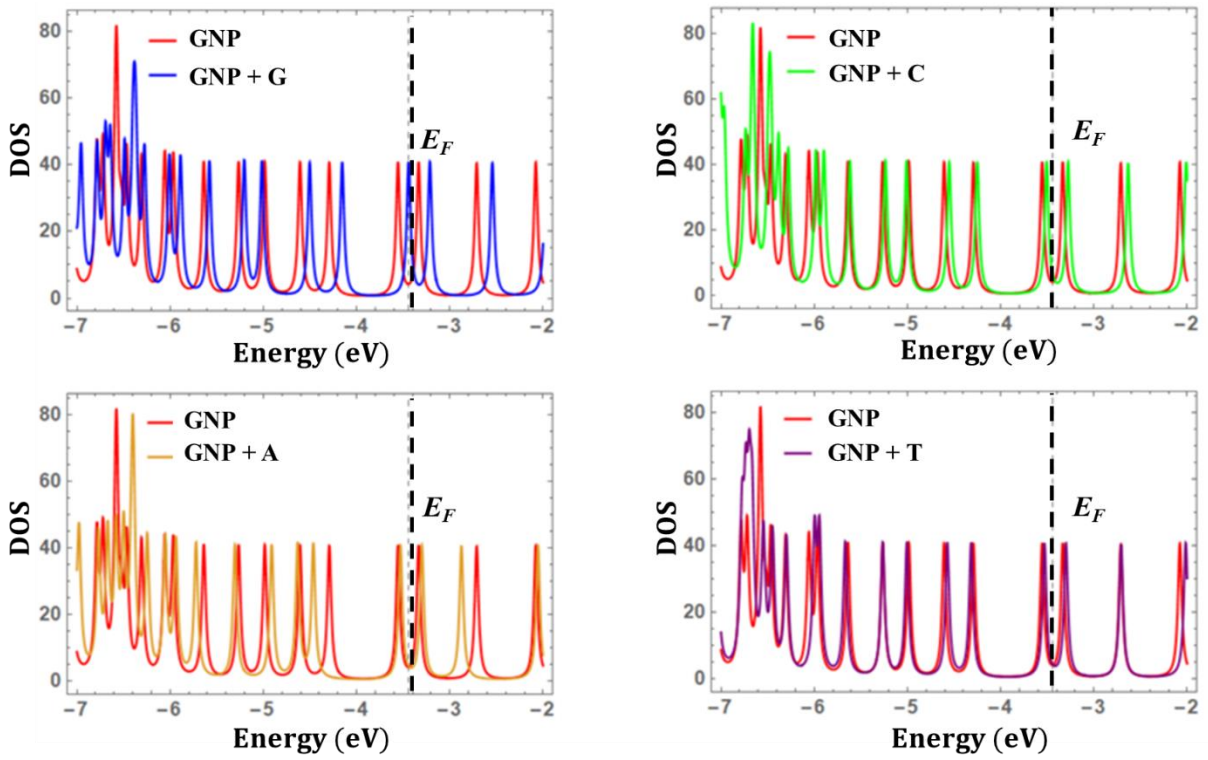


*Figure 21: Density of States plot for GNP systems.*

In agreement with the previous study [3], it is reasonable to determine that GNP systems would not be a suitable candidate for resolving single DNA bases. For instance, the change in energy band gap is minimal for different bases, and the binding energy is large. The DOS shows minimal change as well, suggesting no change in the current. This means tunneling current signal will be indistinguishable for each base.

A similar process can be performed to provide information about the adsorption of DNA bases to a GNR and will be further explored in the following section.

### 4.2 Graphene Nanoribbon (GNR)

Another system of interest is the adsorption of a DNA base to a small GNR, a process called physisorption. As proposed in [3], a small electronic device could be designed to resolve single DNA bases by a process called physisorption. In physisorption a DNA base moves near the surface of the inert GNR and a relatively weak interaction occurs [9]. Studies of the physisorption of DNA nucleobases to inert materials yields information about the binding strength of DNA. It is possible to perform a DFT study on such a system to determine the changes invoked by the presence of

each DNA base. By measuring the changes due to the interaction, it is possible to resolve single DNA bases. The length of the GNR needs to be small enough to restrict interactions to one base at a time. The following section explains the process of modeling the structure of the device.

### 4.2.1 Creating the Graphene Nanoribbon Structure

The structure of the GNR is created in a similar process to the GNP. Nanotube Modeler is used to create the main structure. A GNR of 4W by 3T (1.142 nm by 1.353 nm) is generated to ensure that the largest DNA base fits above the surface without interacting with multiple bases. The distance between bases in a ssDNA is 0.63 nm on average [40] and the largest base, guanine, measures to 0.754 nm at its widest.

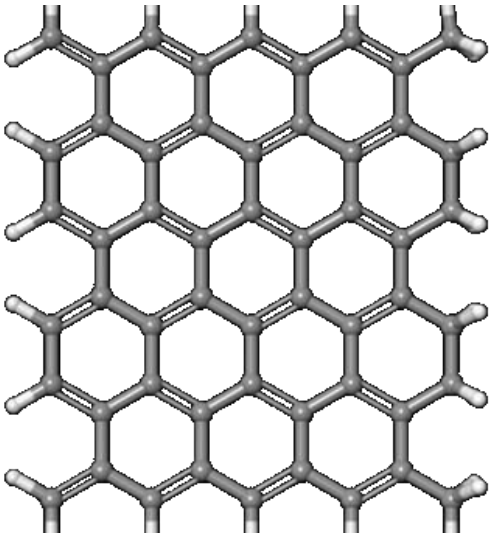

*Figure 22: Initial GNR for physisorption calculation.*

The structure is saved in XYZ file format and opened in Maestro. Once in the Maestro software, Hydrogen atoms are added to the edges to neutralize the charge imposed by dangling bonds. The DNA base structures are then merged with the GNR to create each system. DNA bases are placed parallel to the surface of the GNR at a height of ~ 0.3 nm. The height was determined based on a suggestion from a previous study [9].

Once each structure is complete, input files can be created. Input files for calculations of the following structures were created and studied: GNR, GNR + Adenine, GNR + Guanine, GNR + Cytosine, and GNR + Thymine. An example adenine structure is seen in **Figures 23 & 24** below.

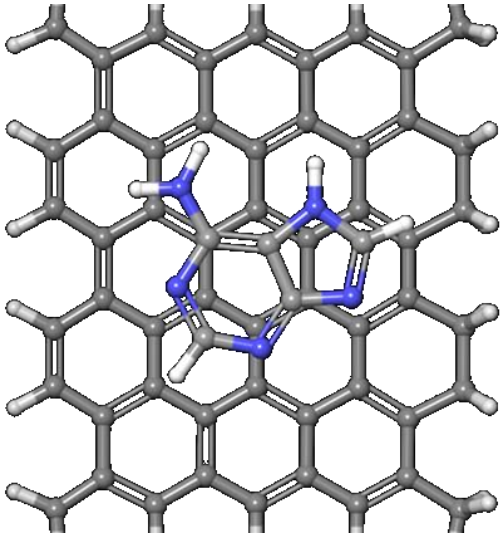

*Figure 23: Adenine + GNR structure ready for calculation (top view).*

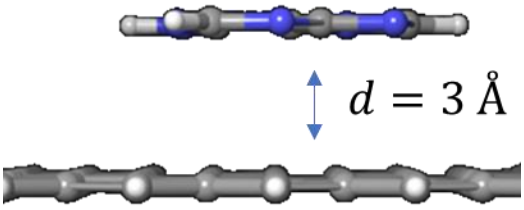


*Figure 24: Adenine + GNR structure ready for calculation (side view).*

### 4.2.2 Creating Graphene Nanoribbon Input Files

Avogadro is once again used to create the input file template. The XYZ file is loaded into Avogadro and the Gaussian Input Generator tool is used to create an input file with the B3LYP/6-31G(d,p) basis set. The SCF convergence criteria is set to SCF = QC. Below the input are the XYZ coordinates of the system. Once the input file is saved in the *filename*.com format in the running directory, one can create the batch script file and run the calculation.

### 4.2.3 Running Graphene Nanoribbon Calculations

Calculations are performed using the Buddy super-computer at the University of Central Oklahoma. Buddy requires SLURM formatted batch script files to submit jobs. Once one batch script file is working, it is possible to tweak the computer parameters to suit the calculation. For GNR physisorption calculations, less nodes were used to accommodate the smaller system, however it is typically faster to use more.

The batch script file should then be saved to the running directory. Using Buddy command line, one navigates to the running directory and submits the job with the command *sbatch filename.sh.* Each calculation varies in length, but **Table 8** below shows runtimes for each system. Note the table does not include queue times.

*Table 8: Nodes, convergence criteria, and runtime for GNR systems.*

| System | Number of Nodes | Convergence Criteria | Runtime (hours) |
|---|---|---|---|
| **GNR + Guanine** | 6 | QC | 47.5 |
| **GNR + Adenine** | 6 | QC | 26.2 |
| **GNR + Cytosine** | 6 | QC | 16.6 |
| **GNR + Thymine** | 6 | QC | 14.5 |
| **GNR** | 3 | QC | 0.6 |

### 4.2.4 Nanoribbon Results

Results are stored in a file with the name *output.log* in the running directory. Key information in the output file includes the final energy, the final energy levels, and the final geometry. It is important to note the confirmation of convergence and the confirmation that Gaussian terminated normally. Information from the output file is analyzed using Mathematica and Microsoft Excel. The following sections outline information obtained about the energy gap, the binding energy, and the density of states.

### 4.2.4 (a) Binding Energy for GNR with DNA Bases

It is also beneficial to calculate the binding energy, as performed in [9]. Given the energy of each the GNR, the combined system, and the DNA base, one can calculate the binding energy of the system:

$$E_{bind} = E_{GNR+base} - (E_{GNR} + E_{base}) \quad \textbf{(5)}$$

where $E_{bind}$ is the binding energy of the system, $E_{GNR+base}$ is the total energy of the combined system (GNR + Base), $E_{GNR}$ is the total energy of the GNR, and $E_{DNA}$ is the total energy of the DNA base. The binding energy is a key parameter that describes the strength of the interaction between the DNA base and the GNR. It was reported in [9] that the binding energy results for graphene yield

G > A ~ C ~ T. Our study shows G > C > A > T. **Table 9** below contains the binding energy and final total energy of each combined systems.

*Table 9: Total energy, energy gap, and binding energy for GNR systems.*

| | $\mathbf{E_{tot}}$ **(eV)** | $\mathbf{E_{gap}}$ **(eV)** | $\mathbf{E_{bind}}$ **(eV)** |
|---|---|---|---|
| **GNR + Guanine** | $-7.119 \times 10^4$ | 0.260 | -0.592 |
| **GNR + Adenine** | $-6.915 \times 10^4$ | 0.257 | -0.546 |
| **GNR + Cytosine** | $-6.718 \times 10^4$ | 0.262 | -0.578 |
| **GNR + Thymine** | $-6.879 \times 10^4$ | 0.258 | -0.423 |

**Figure 25** below shows the binding energy and energy gap for GNR systems. The high binding energies reveal that there could be an issue with the bases sticking to the surface of the GNR. The relatively small changes in the energy gap as bases are toggled also do not yield promising results.

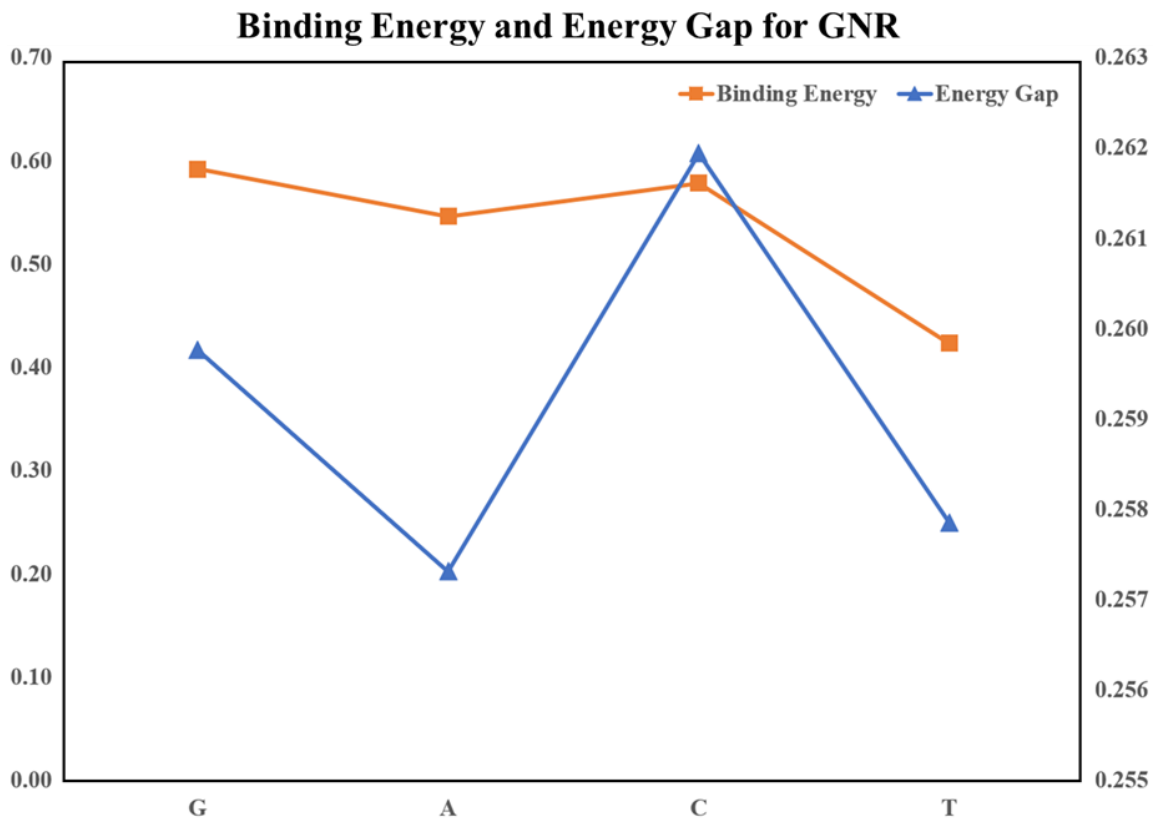


*Figure 25: Plot of Binding energy and energy gap vs. DNA base.*

### 4.2.4 (b) Optimized Geometry for GNR with Different DNA Bases

**Figure 26** below contains illustrations of the final geometry of each combined GNR system with respective binding energies and final distances from the surface. The initial distance was 3.00 Å.

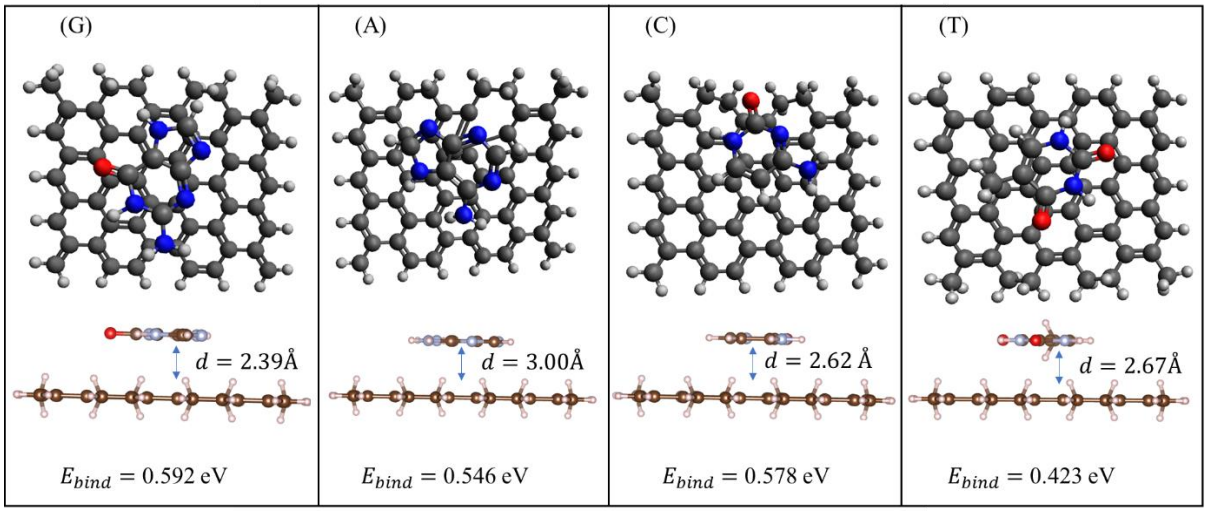


*Figure 26: Optimized geometries of GNR systems with binding energy.*

### 4.2.4 (c) Energy Band Gap for GNR with DNA Bases

**Table 10** below outlines each structure's calculated energy gap. As seen in results from the GNP calculations, there is not a significant change in the energy gap due to the presence of different bases.

*Table 10: Energy Gap for GNR Systems.*

| | **LUMO (eV)** | **HOMO (eV)** | **$E_{gap}$ (eV)** |
|---|---|---|---|
| **GNR + Guanine** | -3.318 | -3.578 | 0.260 |
| **GNR + Adenine** | -3.481 | -3.738 | 0.257 |
| **GNR + Cytosine** | -3.296 | -3.557 | 0.262 |
| **GNR + Thymine** | -3.397 | -3.655 | 0.258 |

### 4.2.4 (d) Density of States for GNR with DNA Bases

It can also be beneficial to plot the density of states to provide visual assistance in determining the practicality of the device for resolving single DNA bases. **Figure 27** below contains the DOS plots for each GNR system.

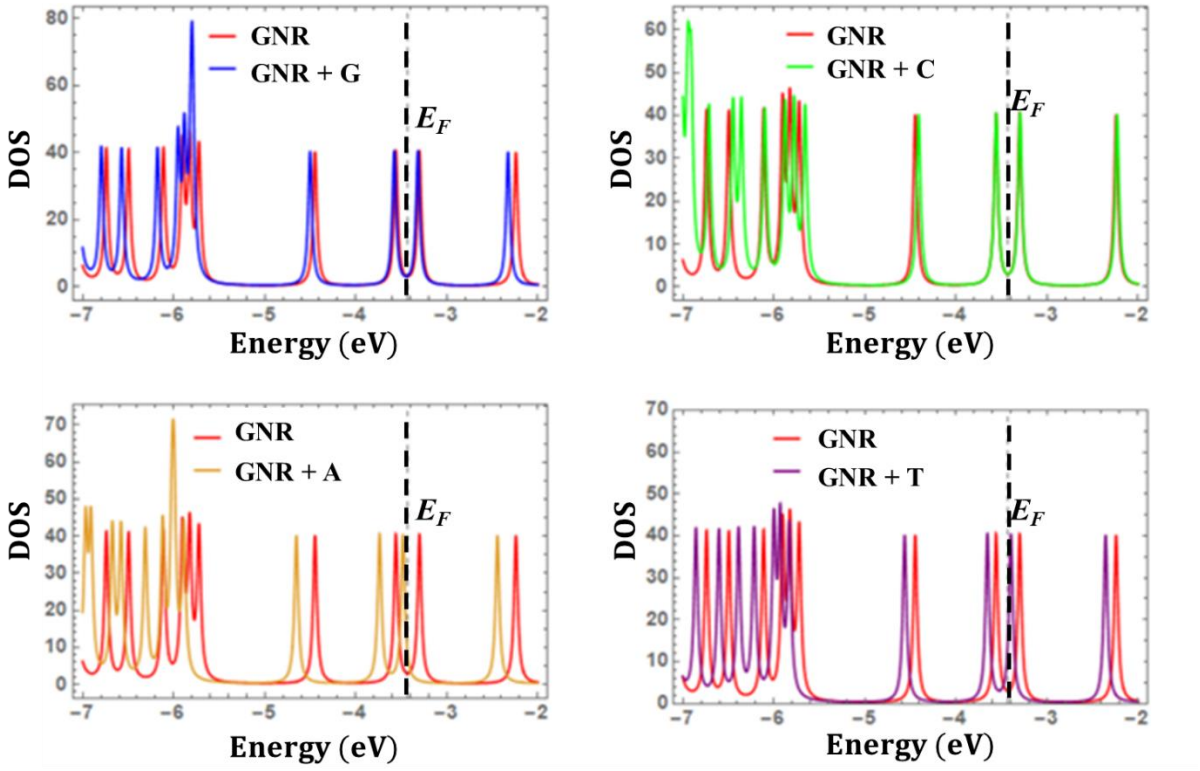


*Figure 27: Density of States plot for GNR.*

The current is proportional to the DOS. The visual assistance provided by the DOS plots provides clear evidence that the system is not varying greatly when toggling each DNA Base, therefore we would expect a miniscule change in the current for a real device.

With a similar result to the GNP study, it is reasonable to conclude that this device would not be suitable for resolving individual DNA bases. Although graphene devices seem to be less than favorable for DNA sensing, other materials may be successful candidates. The next section details a study of the phosphorene nanopore and nanoribbon systems.

# Chapter 5. Interaction of Phosphorene Nanomaterials with DNA Bases

Monolayer black phosphorus, otherwise known as phosphorene, is a 2D material made up entirely of phosphorus atoms and was first synthesized in 2014 by exfoliation of bulk black phosphorus [14]. Bulk black phosphorus (BP) was first obtained in 1914 by conversion from white phosphorus at high temperature and pressure [29]. Unlike the very popular 2D material graphene, which is planar, the phosphorene structure has a puckered appearance along the armchair direction and dual layer appearance on the zigzag side. The structure of phosphorene is made up of phosphorus atoms interconnected to form three bonds each. The remaining lone pair on each atom leads to $sp^3$ hybridization, which is responsible for the puckered surface [18].

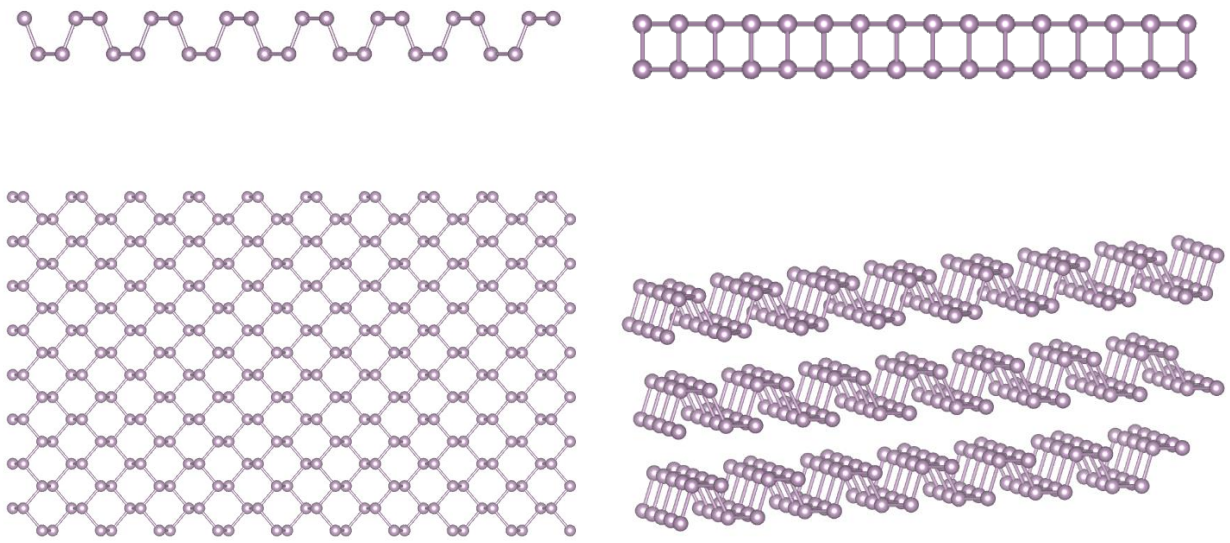

*Figure 28: (top left) Armchair side view of phosphorene, (top right) zigzag side view of phosphorene, (lower left) top view of phosphorene, and (lower right) structure of black phosphorus.*

There are two bond lengths for phosphorene, one between each nearest atom in plane, and one between the upper and lower set of atoms. The in-plane bond length is 0.222 nm, and the between surface bond length is 0.224 nm [14]. If the structure were not puckered, it would present with a more traditional honeycomb lattice crystal structure like the structure of graphene. A top view, zigzag side view, and armchair side view of the structure is seen in **Figure 28** above.

Phosphorene shares many of the remarkable properties of graphene including high carrier mobility [30] and tunable optical properties [32]. The advantage of phosphorene is its direct band gap [31]

that is dependent on thickness, making phosphorene ideal for electronic and optoelectronic applications [33]. The similarities between phosphorene and graphene may come as a surprise due to carbon and phosphorus, the atoms that make up graphene and phosphorene, being in different groups on the periodic table.

*Table 11: Periodic table excerpt of key elements.*

| | | | |
|---|---|---|---|
| 5<br>**B** | 6<br>**C** | 7<br>**N** | 8<br>**O** |
| 13<br>**Al** | 14<br>**Si** | 15<br>**P** | 16<br>**S** |
| 31<br>**Ga** | 32<br>**Ge** | 33<br>**As** | 34<br>**Se** |

The combination of the structure and the properties of phosphorene make it unique in the landscape of new 2D materials [29]. Unfortunately, due to the lone pair in the structure, there is question into the stability of phosphorene in ambient conditions [34]. There are several methods of synthesizing phosphorene such as mechanical exfoliation [35] (the scotch tape method), liquid phase exfoliation which is scalable and more affordable than mechanical exfoliation [36], as well as plasma treatment or laser irradiation [37].

Given the extensive research into graphene as a biosensing device, further study on phosphorene for the same purpose is warranted. Recent studies of a plethora of 2D materials for biomedical applications have been performed such as graphene [2], hexagonal boron nitride [9], and molybdenum disulfide [3] to determine their proficiency at DNA base detection. Phosphorene has received little notice as it is a relatively new material [29]. Phosphorene's large direct band gap provides reason to believe that there may be an advantage in resolving single DNA bases over graphene and other materials.

It is the purpose of this study to explore phosphorene in the same manner that graphene was studied in the previous chapter. The intention is to improve understanding about phosphorene as a DNA nucleobase detector in comparison with graphene. Information about the effectiveness of the material will be obtained through a DFT study. Proposed structures to be studied include: (a) phosphorene nanopore (PNP) for a device that would measure the in plane tunneling current across

a nanopore, and (b) the phosphorene nanoribbon for a device that measures the modulation in current of the nanoribbon due to the adsorption of a DNA base to the 2D surface. The following section outlines results obtained through our own research, performing a DFT study of the phosphorene nanopore (PNP).

## 5.2 Phosphorene Nanopore

### 5.2.1 Creating the Phosphorene Nanopore Structure

The initial phosphorene nanoribbon (PNP) structure was created using the software package Vesta [38]. Vesta allows the user to take a unit cell of a crystal and extend it in three dimensions. Because phosphorene is a derivative of black phosphorus, the unit cell for BP was downloaded from the America Mineralogist Crystal Structure Database website [39]. The unit cell file is opened in Vesta and the boundary function is used to extend the unit cell in three dimensions. The initial structure is X = 10, Y = 1, and Z = 10 see images.

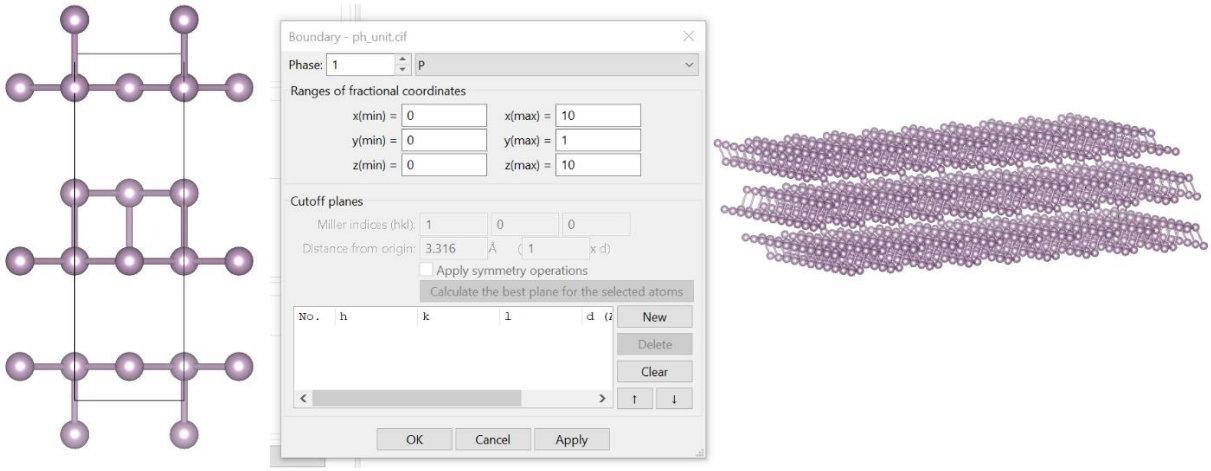


*Figure 29: (left) Unit cell for black phosphorus, (right) Vesta boundary dialog box and structure produced.*

The selection pointer is used to select the bottom and top layers of the BP crystal, which are then deleted. The remaining product is a monolayer of black phosphorus.

The phosphorene structure is exported in XYZ format to be modified in the Maestro software. Once opened in Maestro, the PNR is reduced in size to dimension 7W by 4T to ensure enough space for both a nanopore and DNA base. Hydrogen atoms are added to the edges to neutralize dangling bonds. Recall, the largest DNA base Guanine has maximum width 0.754 nm. Guanine is selected and merged with the PNR structure. The guanine molecule is placed atop the PNR, and phosphorus atoms are deleted to ensure guanine in all orientations fits within the pore. The pore

diameter measures about 1.1 nm, which is on par with the GNP structure and the suggested pore size in [2]. Hydrogen atoms are added inside the pore edges. The guanine is then removed from the structure and the final PNP is remaining. The PNP structure's XYZ file is saved. DNA bases Adenine, Guanine, Cytosine and Thymine are then merged with the PNP structure and placed planar to the 2D surface. With each base placed as nearly as possible to the center of the PNP, XYZ files are exported. Saved structures for calculations include PNP, PNP + Adenine, PNP + Cytosine, PNP + Guanine, and PNP + Thymine. A sample of the PNP + Adenine system is seen in **Figure 30** below.

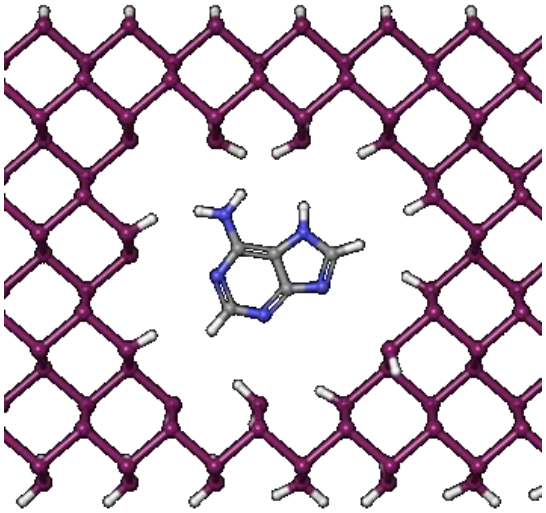

*Figure 30: Structure of PNP + Adenine.*

### 5.2.2 Creating Phosphorene Nanopore Input Files

The software package used to run computations for this study is known as Gaussian 16 [27]. Gaussian requires that input files be created to set parameters, load settings, and provide the structure for each computation. Input files for Gaussian are of the file type *filename.com.* Even though input files can be created from scratch, it is beneficial to use Avogadro software's input file generator to create templates of each input file. Avogadro is a molecular editor but has proven to be a reliable input file generator for Gaussian.

The Avogadro generated input file is altered to include additional settings. Each input file contains a section for computational information, followed by a section that loads the XYZ structure of the studied device. The basis-set B3LYP/6-31G(d,p) was chosen as the most fitting approximation for our system (see DFT chapter for details). After the basis-set selection, the type of calculation is set

as ‘Opt’ which is short for ‘geometry optimization’. Lastly, it is often useful to place SCF = QC or SCF = XQC in the input file to deal with difficult to converge structures (see DFT section). For this computation SCF = XQC was chosen. The input instructions are accompanied by the XYZ coordinates of structure. The file is saved to the running directory (the folder in which the job will be submitted from) as the file type *filename*.com.

### 5.2.3 Running Phosphorene Nanopore Calculations

Calculations are submitted to Buddy super-computer at the University of Central Oklahoma. Buddy requires SLURM formatted batch script files to submit jobs. With working batch script files remaining from running graphene calculations, it is only necessary to tweak the file to suit the PNP calculation.

Although it is typically faster to use more nodes, a resource restriction limiting 9 total nodes maximum be used at any given time was imposed. A table of runtimes for each system is seen below. Note the table does not include queue times.

*Table 12: Nodes, convergence criteria, and runtime for each PNP system.*

| System | Number of Nodes | Convergence Criteria | Runtime (hours) |
|---|---|---|---|
| **PNP + Guanine** | 3 | XQC | 13.5 |
| **PNP + Adenine** | 3 | XQC | 10.9 |
| **PNP + Cytosine** | 3 | XQC | 12.6 |
| **PNP + Thymine** | 3 | XQC | 16.2 |
| **PNP** | 3 | XQC | 11.4 |

Batch script files are saved to the running directory as *filename.sh.* Using the command line to navigate to the running directory, jobs are submitted to Buddy by with the command *sbatch filename.sh*. It is essential that input and batch script files are saved to the same directory as where the job is submitted from.

### 5.2.4 Phosphorene Nanopore Results

Results are stored in a file named *output.log* in the running directory. Key information analyzed in the output file includes the final energy, the final energy levels, and the final geometry.

To ensure that the job ran successfully, it is important to locate 'NORMAL TERMINATION OF GAUSSIAN' at the end of the output file. To ensure successful convergence, it is important to locate the 'CONVERGED' section, where 'YES' dominates each category: maximum force, RMS force, maximum displacement, and RMS displacement. Information from the output file is analyzed using Mathematica and Microsoft Excel. The following sections outline information about the energy gap, the binding energy, and the density of states.

### 5.2.4 (a) Binding Energy for PNP with DNA Bases

It is also beneficial to calculate the binding energy, as performed in [9]. Given the energy of each the PNP, the combined system, and the DNA base, one can calculate the binding energy of the system:

$$E_{bind} = E_{PNP+base} - (E_{PNP} + E_{base}) \quad \textbf{(6)}$$

where $E_{bind}$ is the binding energy of the system, $E_{PNP+base}$ is the total energy of the combined system, $E_{PNP}$ is the total energy of the PNP, and $E_{DNA}$ is the total energy of the DNA base. The binding energy is a key parameter that describes the strength of the interaction between the DNA base and the PNP. In the graphene nanopore study, the binding energy for each base showed C > A > G > T. **Table 13** below contains the binding energy and final total energy of each combined systems. Our study shows that C > G > A > T.

*Table 13: Total energy, energy gap, and binding energy for PNP systems.*

| **System** | **$E_{tot}$ (eV)** | **$E_{gap}$ (eV)** | **$E_{bind}$ (eV)** |
|---|---|---|---|
| **PNP + Guanine** | $-1.074 \times 10^6$ | 3.083 | -0.395 |
| **PNP + Adenine** | $-1.072 \times 10^6$ | 2.789 | -0.307 |
| **PNP + Cytosine** | $-1.070 \times 10^6$ | 3.046 | -0.405 |
| **PNP + Thymine** | $-1.072 \times 10^6$ | 3.025 | -0.200 |

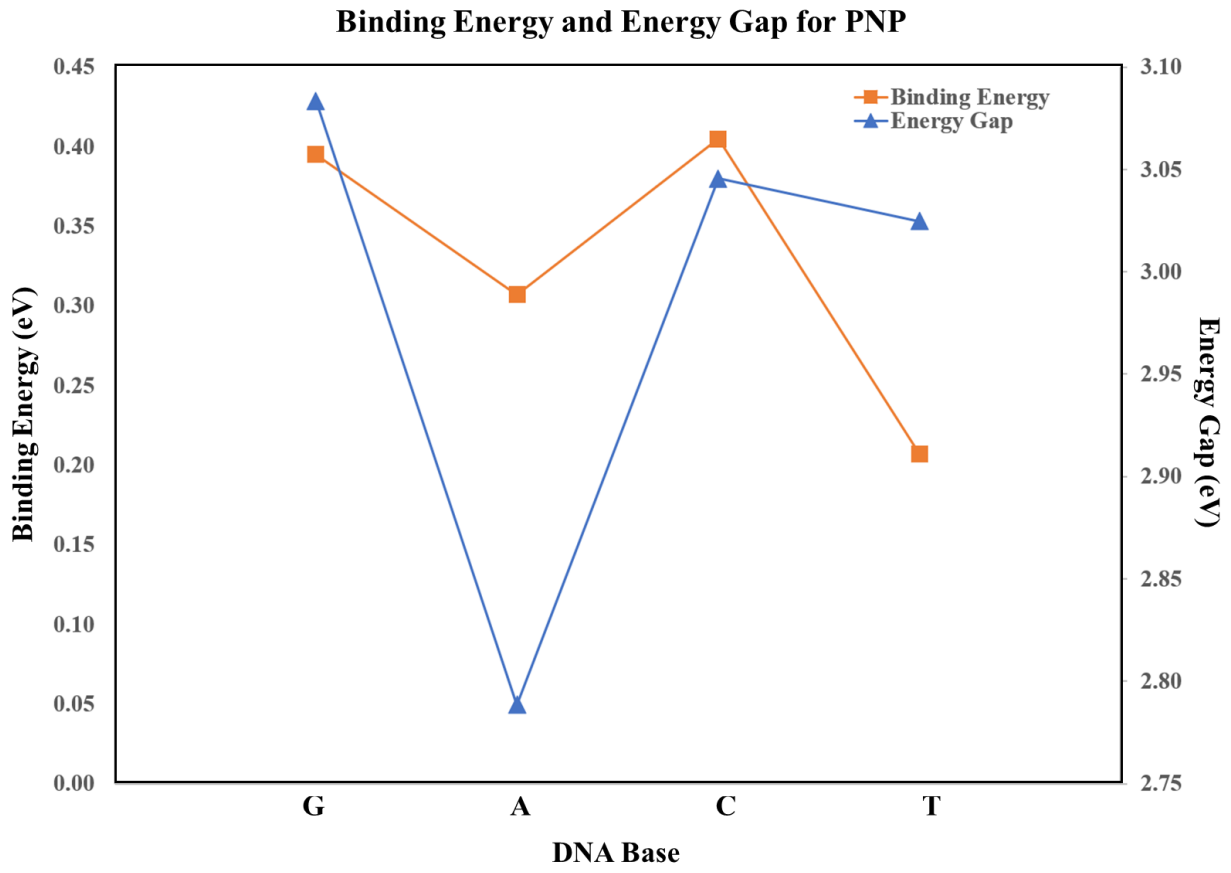


*Figure 31: Binding energy and energy gap of PNP systems.*

**Figure 31** above contains the binding energy and energy gap changes for each combined PNP system. The changes in energy gap are larger than for our graphene systems results. The binding energy is also quite lower than that of graphene and insists that there would be reduced issues with the bases sticking to the pore.

### 5.2.4 (b) Optimized Geometry for PNP with Different DNA Bases

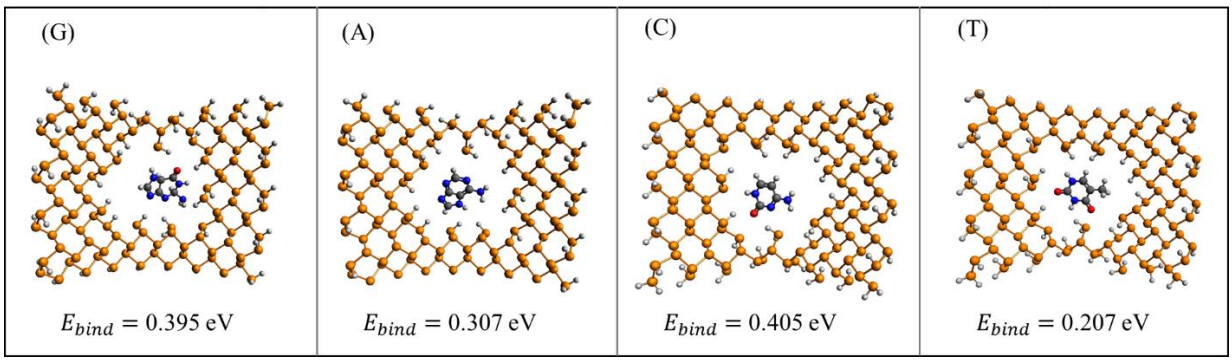


*Figure 32: Optimized geometry of PNP systems and binding energy.*

**Figure 32** provides illustration of the optimized geometry of PNP systems along with the binding energy. The binding energies reported are less than what was discovered for graphene nanopore systems.

### 5.2.4 (c) Energy Band Gap for PNP with DNA Bases

**Table 14** below outlines each structure's calculated energy gap. Note that the energy gap is much larger than that of graphene.

*Table 14: Energy gap for each PNP system.*

| System | LUMO (eV) | HOMO (eV) | $E_{gap}$ (eV) |
|---|---|---|---|
| **Pore** | -2.590 | -5.660 | 3.070 |
| **PNP + Guanine** | -2.586 | -5.670 | 3.083 |
| **PNP + Adenine** | -2.668 | -5.456 | 2.789 |
| **PNP + Cytosine** | -2.682 | -5.728 | 3.046 |
| **PNP + Thymine** | -2.652 | -5.677 | 3.025 |

However, as seen above, there is little change in the energy gap due to the toggling of each DNA base making it difficult to resolve each base.

### 5.2.4 (d) Density of States for PNP with DNA Bases

It is also helpful to generate a density of states plot to provide visual assistance in determining the abilities of each device for resolving individual bases. Below are DOS plots for each system and a final combined DOS plot.

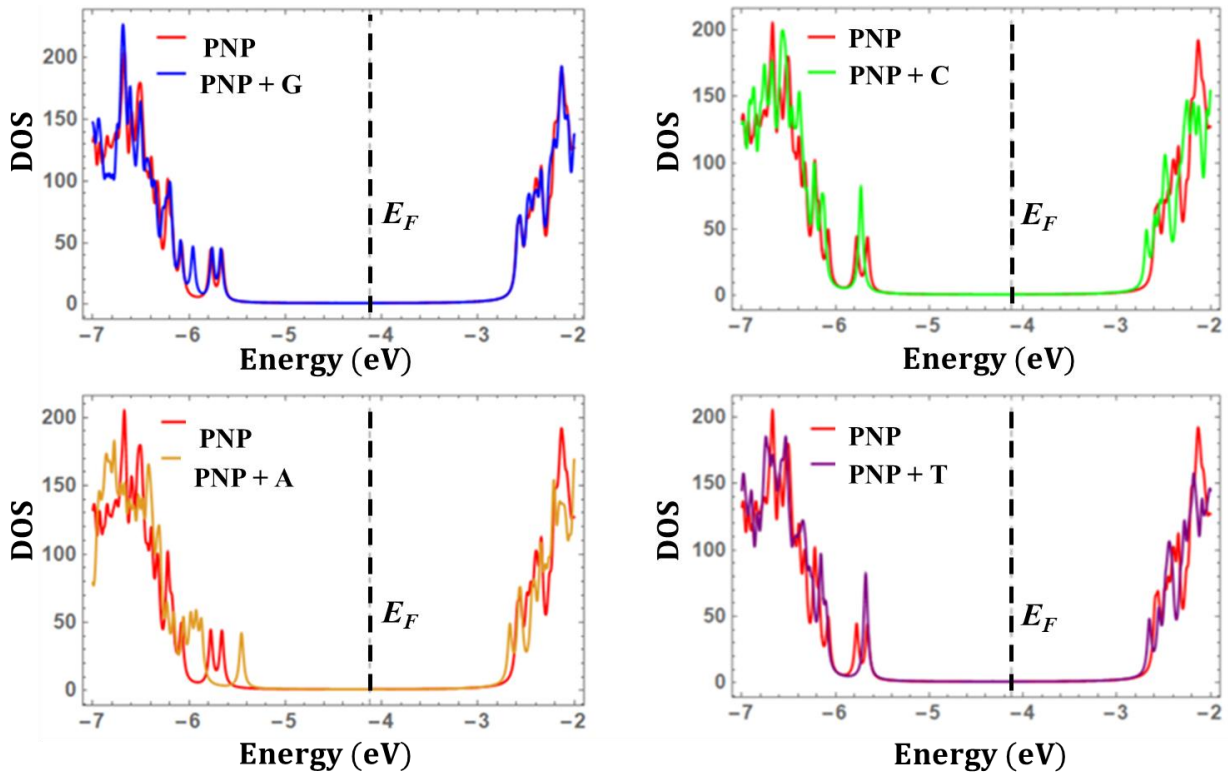


*Figure 33: Density of States plot for PNP.*

As explained in the introduction, a change in the DOS is proportional to changes in current. The small changes in the DOS plot above do not suggest a significant modulation in current. This result is slightly better than that of GNP. The band gap is also evident in the DOS plot and although the band gap is larger for phosphorene, there remains only a small change when due to each DNA base. This makes it difficult to determine which base is in the pore. The next section outlines the study of a phosphorene nanoribbon for physisorption.

### 5.3 Phosphorene Nanoribbon

An additional device of interest is the adsorption, or physisorption, of a DNA nucleobase to a small phosphorene nanoribbon. As proposed in [3], a system is designed to resolve individual DNA bases by physisorption. Physisorption is the weak interaction between the DNA base and the surface of the PNR [9]. By performing a DFT study on the system, it is possible to determine the changes invoked by the presence of each DNA base. This study of the physisorption of each DNA base to the phosphorene can yield information about the binding strength between the two. The following sections outline the creation of the structure, input files, batch script files, and results.

### 5.3.1 Creating the Phosphorene Nanoribbon Structure

The structure of the PNR is created first by using Vesta. A PNR with dimensions 10W by 10T is generated from the unit cell using the 'boundary' function within the Vesta software. This dimension is chosen to ensure that the final structure can be sculpted from the Vesta generated surface. The XYZ file is saved and opened in the molecular editor software Maestro.

Once in Maestro, the structure is reduced to a 4W by 3T sheet to be large enough to contain guanine (.754 nm at its widest). Because ssDNA has a distance 0.63 nm on average [40] between each base, the structure must also be small enough to resolve the individual bases without leaving any room for interaction with other bases. Hydrogen atoms are added to the edges to neutralize dangling bonds. With the final dimension determined, the XYZ file is exported and saved. Each DNA base is merged with the final PNR structure and set parallel to the 2D surface at 0.3 nm. This height was used to compare with our own DFT study of graphene in the previous section. Respective XYZ files were exported and saved. With each structure created, respective input files should be created. Input files for calculations of the following structures were created: PNR, PNR + Adenine, PNR + Guanine, PNR + Cytosine, and PNR + Thymine. A sample structure of PNP + Adenine is seen in **Figure 34** below.

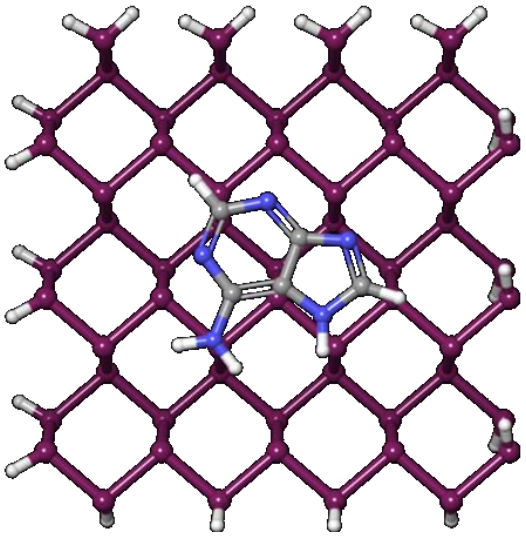

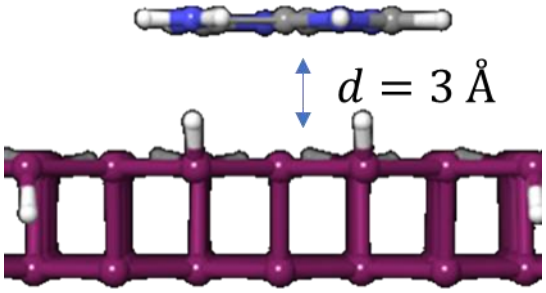


*Figure 34: Top and side views of PNR + Adenine structure ready for calculation.*

### 5.3.2 Creating Phosphorene Nanoribbon Input Files

The software used to perform the DFT calculation is known as Gaussian. To create gaussian formatted input file templates, each structure is loaded into the atomic modeling software Avogadro. The software generates a template that contains the XYZ structure and the computation parameters required by Gaussian. The basis set B3LYP/6-31G(d,p) and is chosen and the keyword 'Opt' is added to run a Geometry Optimization. The SCF convergence criteria is set to SCF = XQC. The input file is saved as *filename*.com in the running directory.

### 5.3.3 Running Phosphorene Nanoribbon Calculations

The DFT calculations are performed using the Buddy super-computer at the University of Central Oklahoma. Buddy requires the user to submit calculations using SLURM formatted batch script files. Once one batch script file is working for a program, the file can be reused by changing the name of the input file. For the PNR physisorption calculations, less nodes were used due to a restriction imposed by the University of Central Oklahoma High Performance Computing Center.

The batch script file is saved to the running directory as *filename.sh*. With the use of the Buddy command line, one navigates to the running directory and submits the job with the command sbatch *filename.sh*. A table of runtimes for each system is seen below. Note the table does not include queue times.

*Table 15: Number of nodes, convergence criteria, and runtimes for each PNR system.*

| System | Number of Nodes | Convergence Criteria | Runtime (hours) |
|---|---|---|---|
| **PNR + Guanine** | 3 | XQC | 7.0 |
| **PNR + Adenine** | 3 | XQC | 14.4 |
| **PNR + Cytosine** | 3 | XQC | 6.8 |
| **PNR + Thymine** | 3 | XQC | 6.4 |
| **PNR** | 3 | XQC | 2.3 |

### 5.3.4 Phosphorene Nanoribbon Results

The results of each calculation are saved to respective output files, *filename.log*, in the running directory. Key information to look for in the output file is the final energy, final energy levels, and the final geometry. The figures below contain sample excerpts of the key output file information.

Note the key information that Gaussian terminated normally and the confirmation of convergence. The output file is analyzed and represented using Microsoft Excel and Wolfram Mathematica. The following sections outline information obtained about the energy gap, the binding energy, and the density of states.

### 5.3.4 (a) Binding Energy for PNR with Different DNA Bases

It is also beneficial to calculate the binding energy, as performed in [9] and our previous calculations. Given the energy of each the PNR, the combined system, and the DNA base, one can calculate the binding energy of the system:

$$E_{bind} = E_{PNR+base} - (E_{PNR} + E_{base}) \quad \textbf{(7)}$$

where $E_{bind}$ is the binding energy of the system, $E_{PNR+base}$ is the total energy of the combined system, $E_{PNR}$ is the total energy of the PNR, and $E_{DNA}$ is the total energy of the DNA base. The binding energy is a key parameter that describes the strength of the interaction between the DNA base and the PNR. Our result from the graphene nanoribbon yielded a binding energy G > C > A > T. **Table 16** below contains the binding energy and final total energy of each combined systems. Our study shows that for PNR physisorption the binding energy trends as G > A > C > T. A similar

result was found for $MoS_2$ in [3] where the binding energy pattern follows G > A > C > T. In [50], researchers found G > A > C > T for phosphorene nanoribbons.

*Table 16: Total energy, energy gap, and binding energy of each PNR system.*

| System | $E_{tot}$ (eV) | $E_{gap}$ (eV) | $E_{bind}$ (eV) |
|---|---|---|---|
| **PNR + Adenine** | $-5.516 \times 10^5$ | 2.783 | -0.293 |
| **PNR + Guanine** | $-5.537 \times 10^5$ | 2.680 | -0.330 |
| **PNR + Cytosine** | $-5.497 \times 10^5$ | 3.022 | -0.189 |
| **PNR + Thymine** | $-5.513 \times 10^5$ | 3.055 | -0.169 |
| **PNR** | $-5.389 \times 10^5$ | 3.038 | x |

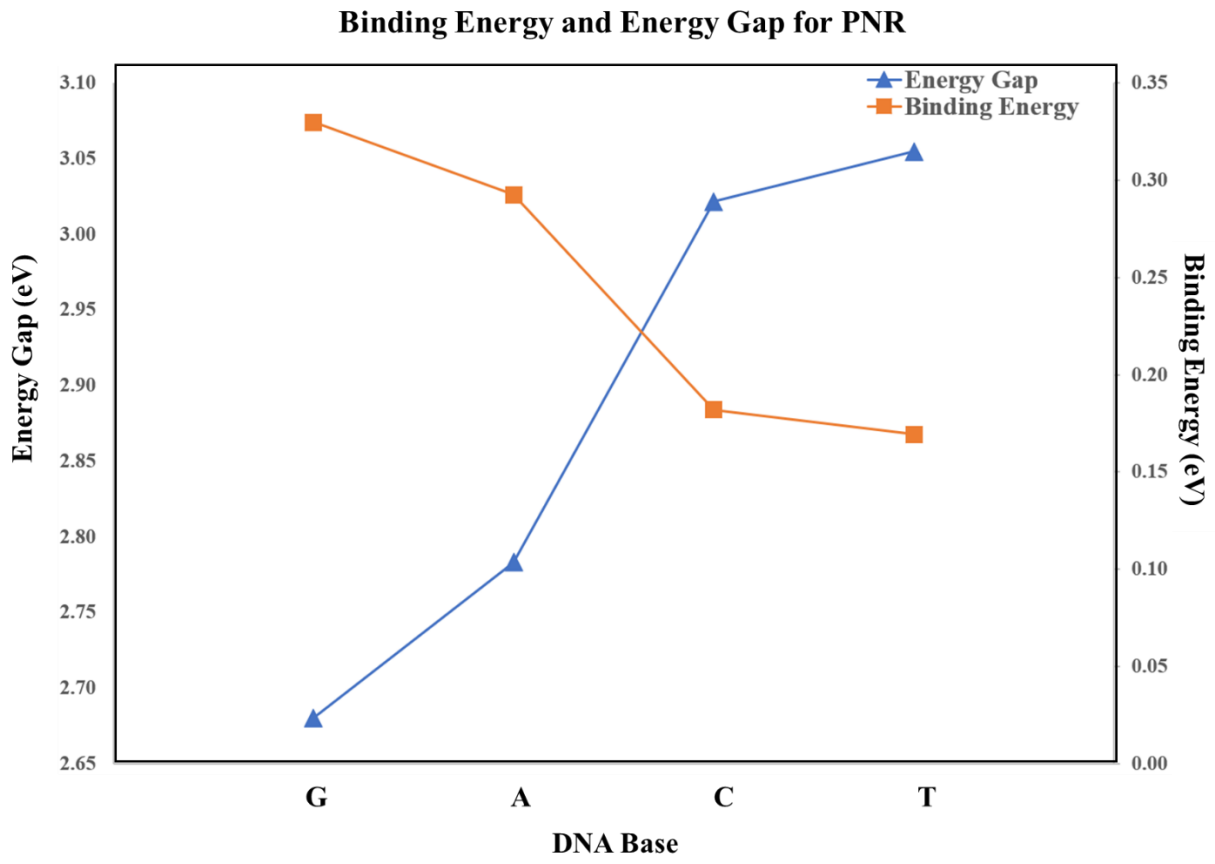


*Figure 35: Energy gap and Binding energy vs. DNA base for each PNR system.*

**Figure 35** above displays the binding energy and energy gap changes for each combined PNR system. The changes in energy gap are more significant than for our graphene systems results. The binding energy is also quite lower than that of graphene and insists that there would be reduced issues with the bases sticking to the surface of the material. The pattern exhibited is also consistent with a molybdenum disulfide study in [3], in which the increase in energy gap coincides with a decrease in binding energy.

### 5.3.4 (b) Optimized Geometry for PNR with DNA Bases

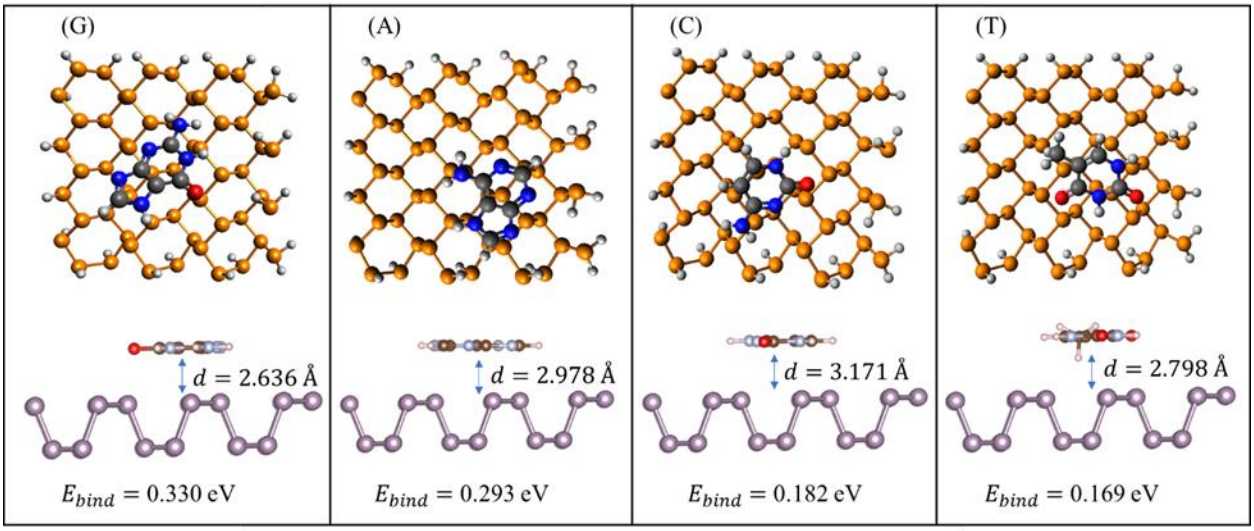


*Figure 36: Optimized geometry of PNR systems with binding energy.*

**Figure 36** above illustrates the final geometries and final minimum distance of the combined PNR structures. Again, the binding energies are lower than what was calculated for graphene leading us to believe that the bases will not display significant sticking to the surface of the PNR. Results in [52] also follow the binding energy order we obtained.

### 5.3.4 (c) Energy Band Gap for PNR with DNA Bases

**Table 17** below outlines each structure's calculated energy gap.

*Table 17: Energy gap for each PNR system.*

| System | LUMO (eV) | HOMO (eV) | $E_{gap}$ (eV) |
|---|---|---|---|
| **PNR** | -2.677 | -5.715 | 3.038 |
| **PNR + Guanine** | -2.768 | -5.448 | 2.680 |
| **PNR + Adenine** | -2.882 | -5.665 | 2.783 |
| **PNR + Cytosine** | -2.623 | -5.645 | 3.022 |
| **PNR + Thymine** | -2.551 | -5.606 | 3.055 |

**Table 17** shows that the energy gap for the PNR + Adenine and PNR + Guanine systems are significantly different from the PNR alone. Unfortunately, there is not as significant of a difference between the PNR and the PNR + Thymine or the PNR + Cytosine system.

### 5.3.4 (d) Density of States for PNR with DNA Bases

It is also beneficial, as in our previous result, to plot the density of states to provide visual assistance in determining the functionality of the structure. Each system's DOS plot was created with the goal to see a significant change in the DOS in the presence of a certain DNA bases. Below are the DOS plots for: PNR + Adenine, PNR + Guanine, PNR + Cytosine, and PNR + Thymine.

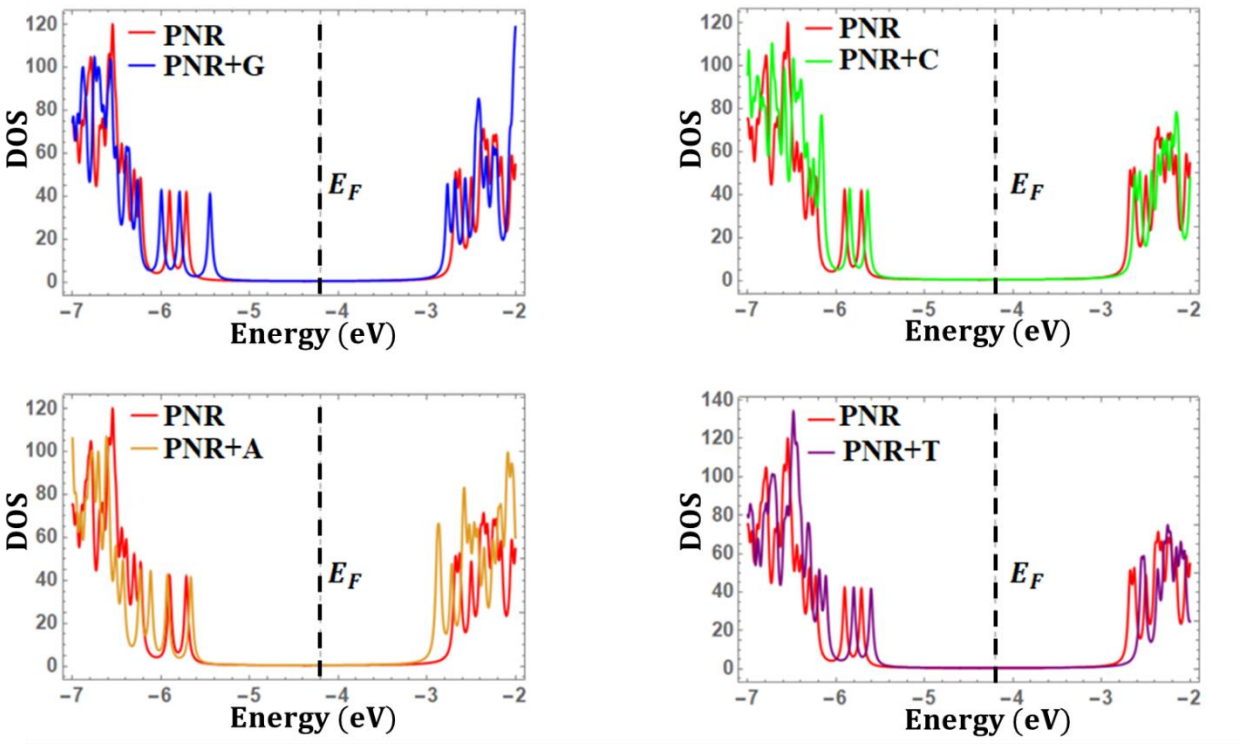


*Figure 37: Density of States for PNR system.*

The DOS plots allow one to visualize how the presence of the DNA base changes the final system. The combined DOS plot shows that there is at least some separation in the PNR + Guanine and PNR + Adenine structures. These modulations in the DOS are directly proportional to the modulations in the current that an experiment would show in the laboratory. Although these modulations are small in the figures above, they are more significant than what is seen in any of the other systems we studied.

These results show that like graphene, there is a small effect due to the presence of each DNA base in the system. However, because the energy gap is much larger in phosphorene, it may be easier to resolve individual bases than using graphene. This is similar to the results seen in [3] for $MoS_2$ where the larger band gap and small binding energies make it a favorable material for DNA base detection.

# Chapter 6. Conclusion, Comparisons, and Perspectives

This research sought to explore the properties of graphene and phosphorene as DNA base detectors by constructing nanopore and nanoribbon systems. The structures were combined with DNA bases and a DFT study was performed. Information on the energy gap, binding energy, and density of states plots were collected for interactions between each DNA base and the respective 2D material.

**Table 18** below outlines a comparison table for the energy gap and binding energy for GNP and PNP systems. Lower binding energies for the PNP structure, as compared to what was calculated for GNP, leads us to suggest that PNP should not exhibit DNA base 'sticking' in the pore. The band gap is also listed, showing that PNP band gaps are significantly smaller than what is found for GNP.

*Table 18: Comparison table of GNP and PNP.*

| | **Band Gap (eV)** | | **Binding Energy (eV)** | |
|---|---|---|---|---|
| **Base** | **GNP** | **PNP** | **GNP** | **PNP** |
| **Pristine** | 0.221 | 3.070 | - | - |
| **G** | 0.228 | 3.083 | 0.888 | 0.395 |
| **A** | 0.230 | 2.789 | 0.936 | 0.307 |
| **C** | 0.230 | 3.046 | 1.063 | 0.405 |
| **T** | 0.231 | 3.025 | 0.871 | 0.207 |

**Table 19** shows the change in energy gap imposed by the presence of each DNA base. The changes in band gap for the GNP system are smaller than the changes in the PNP system. This revelation suggests that PNP systems are more suitable for DNA base detection.

*Table 19: Absolute change in energy gap for GNP and PNP systems due to the presence of DNA base.*

| | $\Delta E_{gap}$ (eV) | |
|---|---|---|
| **Base** | **GNP** | **PNP** |
| **Pristine** | 0 | 0 |
| **G** | 0.007 | 0.013 |
| **A** | 0.009 | 0.281 |
| **C** | 0.009 | 0.024 |
| **T** | 0.010 | 0.045 |

**Figure 38** provides a visual representation of the binding energy differences in GNP and PNP. As previously stated, PNP binding energies are smaller than GNP binding energies.

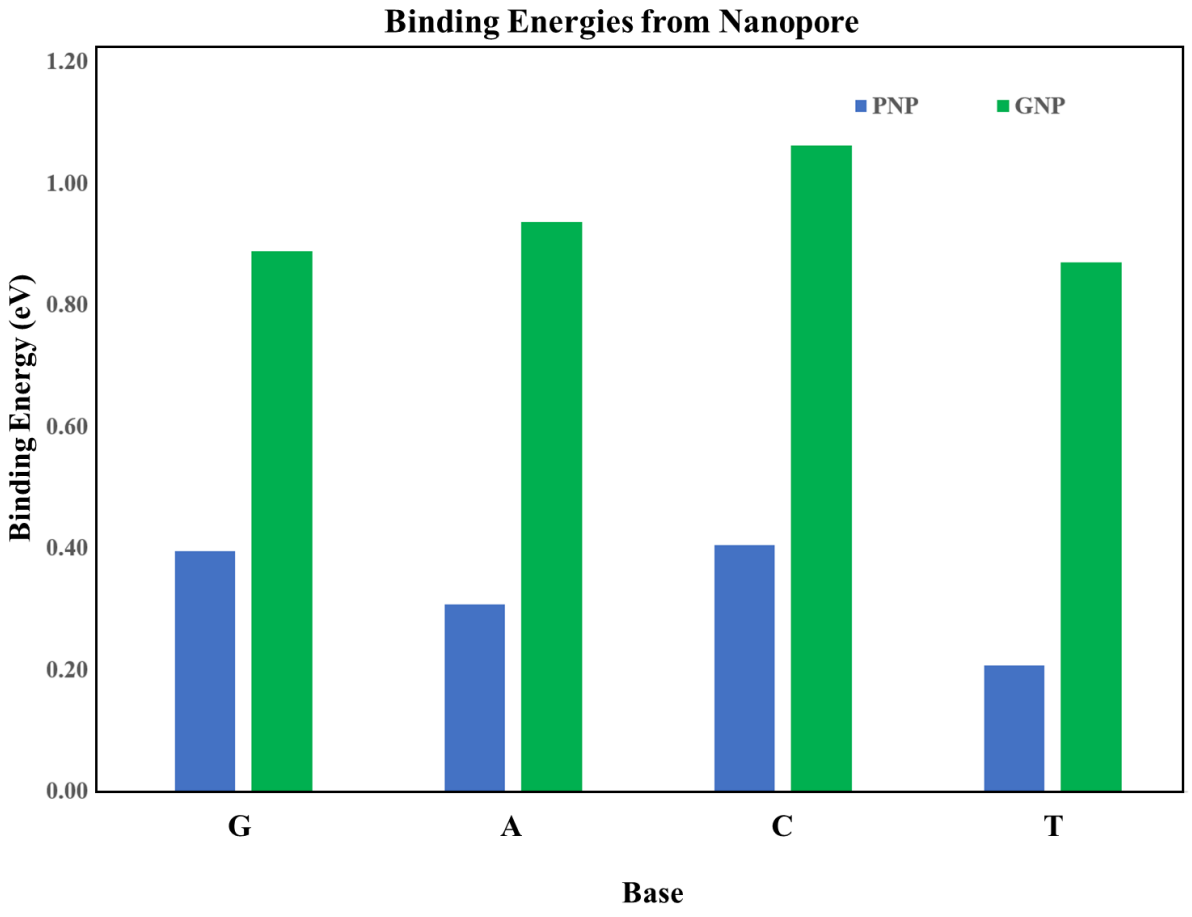


*Figure 38: Visualization of differences in binding energy for PNP and GNP.*

**Table 20** provides comparison between the energy gap and binding energy for GNR and PNR systems. Once again, the band gap is higher for PNR while the binding energy is lower.

*Table 20: Comparison table of GNR and PNR.*

| | Band Gap (eV) | | Binding Energy (eV) | |
|---|---|---|---|---|
| **Base** | **GNR** | **PNR** | **GNR** | **PNR** |
| **Pristine** | 0.259 | 3.038 | - | - |
| **G** | 0.260 | 2.680 | 0.592 | 0.330 |
| **A** | 0.257 | 2.783 | 0.546 | 0.293 |
| **C** | 0.262 | 3.022 | 0.578 | 0.182 |
| **T** | 0.258 | 3.055 | 0.423 | 0.169 |

**Table 21** provides the change in band gap for the GNR and PNR systems.

*Table 21: Absolute change of energy gap for GNR and PNR systems due to the presence of DNA bases.*

| | $\Delta E_{gap}$ (eV) | |
|---|---|---|
| **Base** | **GNR** | **PNR** |
| **Pristine** | 0 | 0 |
| **G** | 0.001 | 0.358 |
| **A** | 0.002 | 0.255 |
| **C** | 0.003 | 0.016 |
| **T** | 0.001 | 0.017 |

**Figure 39** below provides visual comparison of binding energies for PNR and GNR. As previously stated, the binding energy is consistently lower for the PNR than the GNR.

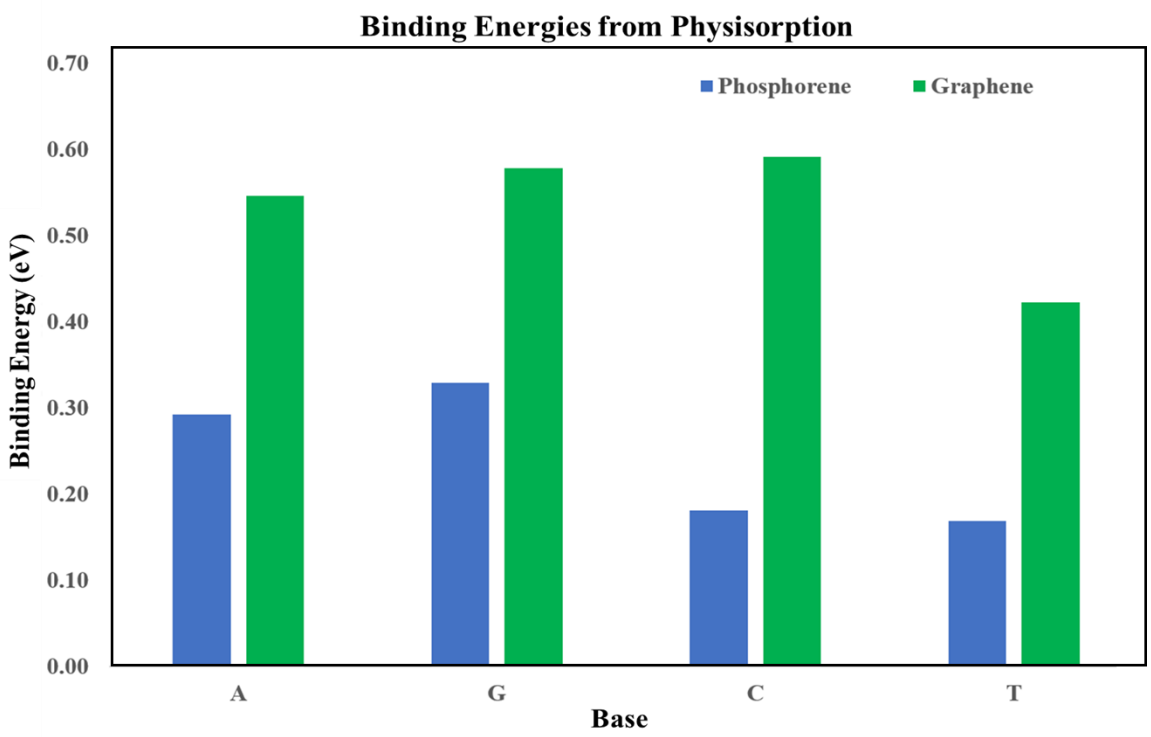


*Figure 39: Binding energies from physisorption for graphene and phosphorene systems.*

In conclusion, it is shown that in comparison with graphene, phosphorene has a larger band gap and displays lower binding energies for each base interaction. DOS results for the phosphorene nanopore show that there are changes imposed by the presence of a DNA base leading to the ability to detect which base is in the pore. Changes in the phosphorene nanoribbon system are supported by a larger change in energy gap and better modulation in DOS plots for each base than what is exhibited by graphene. Maximum energy gap changes for the systems in this study follow the pattern PNR > PNP > GNP > GNR.

The need for solid state device DNA sequencing is strong, and research into new materials and methods is ever increasing [1]. Graphene has been shown to be a promising material, but its issues with pore 'stickiness' and small energy gap has left much to be desired. Our research leads us to predict that phosphorene is a promising material for the future of DNA base detection. We compared our results with similar studies using nanoribbons from $MoS_2$ [3]. Despite the differences in crystal structures of $MoS_2$ and phosphorene, the variation in band gap (G < A < C < T) and binding energies (G > A > C > T) was the same for each material. The change in DOS and band gap for phosphorene for each base was larger compared to $MoS_2$. The binding energies of bases on phosphorene were smaller compared to $MoS_2$. This shows that phosphorene could

perform better as a sequencing material than $MoS_2$. We hope that the findings from this research will serve as a guide to experimentalists and materials scientists working in the field of single-molecule analysis with 2D materials.

Although phosphorene shows improvement over graphene and $MoS_2$, additional studies of phosphorene nanomaterials would be beneficial to extend this research. A periodic calculation of PNR and PNP systems could provide unique insights and perhaps different results to compare with current literature. Studies of other 2D structures, such as transition metal dichalcogenides and van der Waals structures should also be explored in future research.

Our research has opened a door for future computational physics studies at the University of Central Oklahoma. Skills in molecular modeling, computational chemistry software, and data analysis have been molded throughout this project. With the necessary files and theory stated in this thesis, future researchers in Dr. Tayo's research group can extend this study to a greater number of materials.

# References


[1] Prasongkit, Jariyanee, Grigoriev, Anton, Pathak, Biswarup, Ahuja, Rajeev, & Scheicher, Ralph H. (2011). Transverse Conductance of DNA Nucleotides in a Graphene Nanogap from First Principles. *Nano Letters*, **11** (5), 1941-1945.

[2] Heerema, Stephanie J, & Dekker, Cees. (2016). Graphene nanodevices for DNA sequencing. *Nature Nanotechnology*, **11** (2), 127-136.

[3] Farimani, Amir Barati, Min, Kyoungmin, & Aluru, Narayana R. (2014). DNA Base Detection Using a Single-Layer $MoS_2$. *ACS Nano*, **8** (8), 7914-7922.

[4] Heather, James M, & Chain, Benjamin. (2016). The sequence of sequencers: The history of sequencing DNA. *Genomics* (San Diego, Calif.), **107** (1), 1-8.

[5] Ansorge, W. J. (2009). Next-generation DNA sequencing techniques. *New Biotechnology*, **25** (4), 195-203.

[6] Mikheyev, Alexander S, & Tin, Mandy M. Y. (2014). A first look at the Oxford Nanopore MinION sequencer. *Molecular Ecology Resources*, **14** (6), 1097-1102.

[7] Rosenstein, Jacob K, Wanunu, Meni, Merchant, Christopher A, Drndic, Marija, & Shepard, Kenneth L. (2012). Integrated nanopore sensing platform with sub-microsecond temporal resolution. *Nature Methods*, **9** (5), 487-492.

[8] Plesa, Calin, Van Loo, Nick, Ketterer, Philip, Dietz, Hendrik, & Dekker, Cees. (2015). Velocity of DNA during Translocation through a Solid-State Nanopore. *Nano Letters*, **15** (1), 732-737.

[9] Lee, Jun-Ho, Choi, Yun-Ki, Kim, Hyun-Jung, Scheicher, Ralph H, & Cho, Jun-Hyung. (2013). Physisorption of DNA Nucleobases on h-BN and Graphene: VdW-Corrected DFT Calculations. *The Journal of Physical Chemistry C*, **117** (26), 13435-13441.

[10] Branton, Daniel, Deamer, David W, Marziali, Andre, Bayley, Hagan, Benner, Steven A, Butler, Thomas, Schloss, Jeffery A. (2008). The potential and challenges of nanopore sequencing. *Nature Biotechnology*, **26** (10), 1146-1153.

[11] The rise and rise of graphene. (2010). *Nature Nanotechnology*, **5** (11), 755.

[12] Lee, C, Wei, X, Kysar, J. W, & Hone, J. (2008). Measurement of the Elastic Properties and Intrinsic Strength of Monolayer Graphene. *Science (American Association for the Advancement of Science)*, **321** (5887), 385-388.

[13] Novoselov, K. S., Geim, A. K., Morozov, S. V., Jiang, D., Zhang, Y., Dubonos, S. V. & Firsov, A. A. (2004). Electric field effect in atomically thin carbon films. *Science*, **306** (5696), 666-669.

[14] Akhtar, Meysam, Anderson, George, Zhao, Rong, Alruqi, Adel, Mroczkowska, Joanna E, Sumanasekera, Gamini, & Jasinski, Jacek B. (2017). Recent advances in synthesis, properties, and applications of phosphorene. *NPJ 2D Materials and Applications*, **1** (1), NPJ 2D materials and applications, 2017, Vol.1 (1).

[15] Balandin, Alexander A, Ghosh, Suchismita, Bao, Wenzhong, Calizo, Irene, Teweldebrhan, Desalegne, Miao, Feng, & Lau, Chun Ning. (2008). Superior Thermal Conductivity of Single-Layer Graphene. *Nano Letters*, **8** (3), 902-907.

[16] Avouris, P. (2010). Graphene: Electronic and Photonic Properties and Devices. *Nano Letters*, **10** (11), 4285-4294.

[17] Han, Melinda Y, Özyilmaz, Barbaros, Zhang, Yuanbo, & Kim, Philip. (2007). Energy Band-Gap Engineering of Graphene Nanoribbons. *Physical Review Letters*, **98** (20), 206805.

[18] Rodin, A. S, Carvalho, A, & Castro Neto, A. H. (2014). Strain-Induced Gap Modification in Black Phosphorus. Physical Review Letters, **112** (17), 176801.

[19] Paredes, J. I., Villar-Rodil, S., Martínez-Alonso, A. & Tascón, J. M. D. Graphene Oxide Dispersions in Organic Solvents. *Langmuir*, **24**, 10560–10564 (2008).

[20] Luong, Duy X, Bets, Ksenia V, Algozeeb, Wala Ali, Stanford, Michael G, Kittrell, Carter, Chen, Weiyin, Tour, James M. (2020). Gram-scale bottom-up flash graphene synthesis. *Nature (London)*, **577** (7792), 647-651.

[21] Palacios, J. J. (2014). Graphene nanoribbons: Electrons go ballistic. *Nature Physics*, **10** (3), 182.

[22] Garaj, S, Hubbard, W, Reina, A, Kong, J, Branton, D, & Golovchenko, J. A. (2010). Graphene as a subnanometre trans-electrode membrane. *Nature (London)*, **467** (7312), 190-193.

[23] Schneider, Grégory F, Kowalczyk, Stefan W, Calado, Victor E, Pandraud, Grégory, Zandbergen, Henny W, Vandersypen, Lieven M. K, & Dekker, Cees. (2010). DNA Translocation through Graphene Nanopores. *Nano Letters*, **10** (8), 3163-3167.

[24] An algorithm for connecting two arbitrary carbon nanotubes, S. Melchor; J.A. Dobado. *Journal of Chemical Information and Computer Sciences*, **44**, 1639-1646 (2004).

[25] Jmol: an open-source Java viewer for chemical structures in 3D. *http://www.jmol.org/*

[26] Schrödinger Release 2020-3: Maestro, Schrödinger, LLC, New York, NY, 2020.

[27] Gaussian 16, Revision C.01, Frisch, M. J. et al., Gaussian, Inc., Wallingford CT, 2016.

[28] Avogadro: an open-source molecular builder and visualization tool. Version 1.2.0. http://avogadro.cc/

[29] Anju, Surendranath, Ashtami, Jayakumar, & Mohanan, P.V. (2019). Black phosphorus, a prospective graphene substitute for biomedical applications. *Materials Science and Engineering*: C, 97, 978-993.

[30] Wei, Qun, & Peng, Xihong. (2014). Superior mechanical flexibility of phosphorene and few-layer black phosphorus.

[31] Zhou, X. Y, Zhang, R, Sun, J. P, Zou, Y. L, Zhang, D, Lou, W. K, . . . Chang, Kai. (2015). Landau levels and magneto-transport property of monolayer phosphorene. *Scientific Reports*, **5** (1), 12295.

[32] Low, Tony, Rodin, A. S, Carvalho, A, Jiang, Yongjin, Wang, Han, Xia, Fengnian, & Castro Neto, A. H. (2014). Tunable optical properties of multilayer black phosphorus thin films. *Physical Review. B*, **90** (7), 2014.

[33] Chen, Yantao, Ren, Ren, Pu, Haihui, Chang, Jingbo, Mao, Shun, & Chen, Junhong. (2017). Field-effect transistor biosensors with two-dimensional black phosphorus nanosheets. *Biosensors & Bioelectronics*, **89** (Pt 1), 505-510.

[34] Wood, Joshua D, Wells, Spencer A, Jariwala, Deep, Chen, Kan-Sheng, Cho, EunKyung, Sangwan, Vinod K, Hersam, Mark C, et al., (2014). Effective Passivation of Exfoliated Black Phosphorus Transistors against Ambient Degradation. *Nano Letters*, **14** (12), 6964-6970.

[35] Li, Likai, Yu, Yijun, Ye, Guo Jun, Ge, Qingqin, Ou, Xuedong, Wu, Hua, Zhang, Yuanbo. (2014). Black phosphorus field-effect transistors. *Nature Nanotechnology*, **9** (5), 372-377.

[36] Del Rio Castillo, Antonio Esau, Pellegrini, Vittorio, Sun, Haiyan, Buha, Joka, Dinh, Duc Anh, Lago, Emanuele, Bonaccorso, Francesco. (2018). Exfoliation of Few-Layer Black Phosphorus in Low-Boiling-Point Solvents and Its Application in Li-Ion Batteries. *Chemistry of Materials*, **30** (2), 506-516.

[37] Lu, W., Nan, H., Hong, J., Chen, Y., Zhu, C., Liang, Z., Zhang, Z. (2014). Plasma-assisted fabrication of monolayer phosphorene and its Raman characterization. Nano Research, 7(6), 853-859.

[38] K. Momma and F. Izumi, "VESTA 3 for three-dimensional visualization of crystal, volumetric and morphology data," *J. Appl. Crystallogr.*, **44**, 1272-1276 (2011).

[39] Cartz, L., Srinivasa, S. R., Riedner, R. J., Jorgensen, J. D., & Worlton, T. G. (1979). Effect of pressure on bonding in black phosphorus. *The Journal of Chemical Physics*, **71** (4), 1718-1721.

[40] Ambia-Garrido, J, Vainrub, Arnold, & Pettitt, B. Montgomery. (2010). A model for structure and thermodynamics of ssDNA and dsDNA near a surface: A coarse grained approach. *Computer Physics Communications*, **181** (12), 2001-2007.

[41] Daniel Richards, Elif Ertekin, Jeffrey C Grossman, David Strubbe, Justin Riley (2017), "MIT Atomic-Scale Modeling Toolkit," https://nanohub.org/resources/ucb_compnano. (DOI: 10.4231/D3VT1GS0N).

[42] B.M. Bode and M.S. Gordon J. Mol. Graphics and Modeling, 16, 133-138 (1998)

[43] Kilina, Svetlana, Tretiak, Sergei, Yarotski, Dzmitry A, Zhu, Jian-Xin, Modine, Norman, Taylor, Antoinette, & Balatsky, Alexander V. (2007). Electronic Properties of DNA Base

Molecules Adsorbed on a Metallic Surface. *The Journal of Physical Chemistry C*, **111** (39), 14541-14551.

[44] Hasnip, Philip J, Refson, Keith, Probert, Matt I. J, Yates, Jonathan R, Clark, Stewart J, & Pickard, Chris J. (2014). Density functional theory in the solid state. Philosophical Transactions of the Royal Society of London. Series A: Mathematical, Physical, and Engineering Sciences, **372** (2011), 20130270.

[45] Riess, J., & Münch, W. (1981). The theorem of Hohenberg and Kohn for subdomains of a quantum system. *Theoretica chimica acta*, **58** (4), 295-300.

[46] Singh, I., El-Emam, A. A., Pathak, S. K., Srivastava, R., Shukla, V. K., Prasad, O., & Sinha, L. (2019). Experimental and theoretical DFT (B3LYP, X3LYP, CAM-B3LYP and M06-2X) study on electronic structure, spectral features, hydrogen bonding and solvent effects of 4-methylthiadiazole-5-carboxylic acid. *Molecular Simulation*, **45** (13), 1029-1043.

[47] Basis Sets and Psuedopotentials https://www.msg.chem.iastate.edu/tutorials/Basissets.pptx

[48] Thomas, L. (2015, November 12). UCO Supercomputer Celebrated with Ribbon-Cutting. Retrieved August 18, 2020, from https://www3.uco.edu/press/prdetail.asp?NewsID=20505

[49] SCF. (2017, January 05). Retrieved August 18, 2020, from *https://gaussian.com/scf/*

[50] Kumawat, Rameshwar L, & Pathak, Biswarup. (2019). Individual Identification of DNA Nucleobases on Atomically Thin Black Phosphorene Nanoribbons: van der Waals Corrected Density Functional Theory Calculations. *Journal of Physical Chemistry C*, **123** (36), 22377–22383. https://doi.org/10.1021/acs.jpcc.9b06239

[51] Kumawat, R. L., & Pathak, B. (2019). Individual Identification of DNA Nucleobases on Atomically Thin Black Phosphorene Nanoribbons: van der Waals Corrected Density Functional Theory Calculations. *The Journal of Physical Chemistry C*, **123** (36), 22377-22383.

# Appendix A: Sample Input Files

Below is a sample gaussian input file for the GNP + Adenine system. The input file was created using the Avogadro Gaussian input generator tool. Add SCF = QC or SCF = XQC for stronger convergence factor.

#n B3LYP/6-31G(d,p) Opt

Adenine with Pore

0 1

| | | | |
|---|---|---|---|
| N | 14.36530 | 10.95100 | 0.00000 |
| C | 14.85270 | 9.72370 | 0.00000 |
| N | 16.14380 | 9.47570 | 0.00010 |
| C | 17.02850 | 10.47780 | -0.00020 |
| N | 18.37290 | 10.54980 | 0.00030 |
| C | 18.74800 | 11.79870 | 0.00020 |
| N | 17.66580 | 12.60920 | -0.00030 |
| C | 16.55020 | 11.79860 | -0.00060 |
| C | 15.17040 | 12.01030 | -0.00020 |
| N | 14.65090 | 13.29480 | 0.00040 |
| H | 14.16420 | 8.89160 | 0.00020 |
| H | 19.77380 | 12.13650 | 0.00080 |
| H | 17.67280 | 13.57920 | -0.00020 |
| H | 15.24790 | 14.05940 | 0.00060 |
| H | 13.69030 | 13.42950 | 0.00060 |
| C | 8.61440 | 3.55250 | 0.00000 |
| C | 7.38370 | 4.26300 | 0.00000 |
| C | 8.61440 | 6.39450 | 0.00000 |

| | | | |
|---|---|---|---|
| C | 7.38370 | 5.68400 | 0.00000 |
| C | 8.61440 | 7.81550 | 0.00000 |
| C | 7.38370 | 8.52600 | 0.00000 |
| C | 8.61440 | 10.65750 | 0.00000 |
| C | 7.38370 | 9.94700 | 0.00000 |
| C | 8.61440 | 12.07850 | 0.00000 |
| C | 7.38370 | 12.78900 | 0.00000 |
| C | 8.61440 | 14.92050 | 0.00000 |
| C | 7.38370 | 14.21000 | 0.00000 |
| C | 8.61440 | 16.34150 | 0.00000 |
| C | 7.38370 | 17.05200 | 0.00000 |
| C | 8.61440 | 19.18350 | 0.00000 |
| C | 7.38370 | 18.47300 | 0.00000 |
| C | 11.07560 | 3.55250 | 0.00000 |
| C | 9.84500 | 4.26300 | 0.00000 |
| C | 11.07560 | 6.39450 | 0.00000 |
| C | 9.84500 | 5.68400 | 0.00000 |
| C | 11.07560 | 7.81550 | 0.00000 |
| C | 9.84500 | 8.52600 | 0.00000 |
| C | 9.84500 | 9.94700 | 0.00000 |
| C | 9.84500 | 12.78900 | 0.00000 |
| C | 11.07560 | 14.92050 | 0.00000 |
| C | 9.84500 | 14.21000 | 0.00000 |
| C | 11.07560 | 16.34150 | 0.00000 |
| C | 9.84500 | 17.05200 | 0.00000 |
| C | 11.07560 | 19.18350 | 0.00000 |
| C | 9.84500 | 18.47300 | 0.00000 |
| C | 13.53680 | 3.55250 | 0.00000 |

| | | | |
|---|---|---|---|
| C | 12.30620 | 4.26300 | 0.00000 |
| C | 13.53680 | 6.39450 | 0.00000 |
| C | 12.30620 | 5.68400 | 0.00000 |
| C | 13.53680 | 16.34150 | 0.00000 |
| C | 12.30620 | 17.05200 | 0.00000 |
| C | 13.53680 | 19.18350 | 0.00000 |
| C | 12.30620 | 18.47300 | 0.00000 |
| C | 15.99810 | 3.55250 | 0.00000 |
| C | 14.76750 | 4.26300 | 0.00000 |
| C | 14.76750 | 5.68400 | 0.00000 |
| C | 14.76750 | 17.05200 | 0.00000 |
| C | 15.99810 | 19.18350 | 0.00000 |
| C | 14.76750 | 18.47300 | 0.00000 |
| C | 18.45930 | 3.55250 | 0.00000 |
| C | 17.22870 | 4.26300 | 0.00000 |
| C | 18.45930 | 6.39450 | 0.00000 |
| C | 17.22870 | 5.68400 | 0.00000 |
| C | 18.45930 | 16.34150 | 0.00000 |
| C | 17.22870 | 17.05200 | 0.00000 |
| C | 18.45930 | 19.18350 | 0.00000 |
| C | 17.22870 | 18.47300 | 0.00000 |
| C | 20.92060 | 3.55250 | 0.00000 |
| C | 19.69000 | 4.26300 | 0.00000 |
| C | 20.92060 | 6.39450 | 0.00000 |
| C | 19.69000 | 5.68400 | 0.00000 |
| C | 20.92060 | 7.81550 | 0.00000 |
| C | 20.92060 | 14.92050 | 0.00000 |
| C | 20.92060 | 16.34150 | 0.00000 |

| | | | |
|---|---|---|---|
| C | 19.69000 | 17.05200 | 0.00000 |
| C | 20.92060 | 19.18350 | 0.00000 |
| C | 19.69000 | 18.47300 | 0.00000 |
| C | 23.38180 | 3.55250 | 0.00000 |
| C | 22.15120 | 4.26300 | 0.00000 |
| C | 23.38180 | 6.39450 | 0.00000 |
| C | 22.15120 | 5.68400 | 0.00000 |
| C | 23.38180 | 7.81550 | 0.00000 |
| C | 22.15120 | 8.52600 | 0.00000 |
| C | 23.38180 | 10.65750 | 0.00000 |
| C | 22.15120 | 9.94700 | 0.00000 |
| C | 23.38180 | 12.07850 | 0.00000 |
| C | 22.15120 | 12.78900 | 0.00000 |
| C | 23.38180 | 14.92050 | 0.00000 |
| C | 22.15120 | 14.21000 | 0.00000 |
| C | 23.38180 | 16.34150 | 0.00000 |
| C | 22.15120 | 17.05200 | 0.00000 |
| C | 23.38180 | 19.18350 | 0.00000 |
| C | 22.15120 | 18.47300 | 0.00000 |
| C | 24.61240 | 4.26300 | 0.00000 |
| C | 24.61240 | 5.68400 | 0.00000 |
| C | 24.61240 | 8.52600 | 0.00000 |
| C | 24.61240 | 9.94700 | 0.00000 |
| C | 24.61240 | 12.78900 | 0.00000 |
| C | 24.61240 | 14.21000 | 0.00000 |
| C | 24.61240 | 17.05200 | 0.00000 |
| C | 24.61240 | 18.47300 | 0.00000 |
| H | 8.61440 | 20.26350 | 0.00000 |

| | | | |
|---|---|---|---|
| H | 11.07560 | 20.26350 | 0.00000 |
| H | 13.53680 | 20.26350 | 0.00000 |
| H | 15.99810 | 20.26350 | 0.00000 |
| H | 18.45930 | 20.26350 | 0.00000 |
| H | 20.92060 | 20.26350 | 0.00000 |
| H | 23.38180 | 20.26350 | 0.00000 |
| H | 25.54770 | 3.72300 | 0.00000 |
| H | 25.54770 | 6.22400 | 0.00000 |
| H | 25.54770 | 7.98600 | 0.00000 |
| H | 25.54770 | 10.48700 | 0.00000 |
| H | 25.54770 | 12.24900 | 0.00000 |
| H | 25.54770 | 14.75000 | 0.00000 |
| H | 25.54770 | 16.51200 | 0.00000 |
| H | 25.54770 | 19.01300 | 0.00000 |
| H | 6.44840 | 3.72300 | 0.00000 |
| H | 6.44840 | 6.22400 | 0.00000 |
| H | 6.44840 | 7.98600 | 0.00000 |
| H | 6.44840 | 10.48700 | 0.00000 |
| H | 6.44840 | 12.24900 | 0.00000 |
| H | 6.44840 | 14.75000 | 0.00000 |
| H | 6.77070 | 16.69800 | 0.82890 |
| H | 6.77070 | 16.69800 | -0.82890 |
| H | 6.77070 | 18.82700 | 0.82890 |
| H | 6.77070 | 18.82700 | -0.82890 |
| H | 12.01090 | 8.35550 | 0.00000 |
| H | 10.45810 | 10.30090 | 0.82880 |
| H | 10.45810 | 10.30090 | -0.82880 |
| H | 10.45810 | 12.43510 | -0.82880 |

| | | | |
|---|---|---|---|
| H | 10.45810 | 12.43510 | 0.82880 |
| H | 12.01090 | 14.38050 | 0.00000 |
| H | 13.53680 | 7.47450 | 0.00000 |
| H | 13.53680 | 15.26150 | 0.00000 |
| H | 18.45930 | 7.47450 | 0.00000 |
| H | 18.45930 | 15.26150 | 0.00000 |
| H | 20.30750 | 8.16940 | 0.82880 |
| H | 20.30750 | 8.16940 | -0.82880 |
| H | 20.30750 | 14.56660 | -0.82880 |
| H | 20.30750 | 14.56660 | 0.82880 |
| H | 21.21590 | 10.48700 | 0.00000 |
| H | 21.21590 | 12.24900 | 0.00000 |
| H | 15.38050 | 6.03800 | 0.82890 |
| H | 15.38050 | 6.03800 | -0.82890 |
| H | 15.70280 | 16.51200 | 0.00000 |
| H | 16.29340 | 6.22400 | 0.00000 |
| H | 16.61560 | 16.69810 | 0.82880 |
| H | 16.61560 | 16.69810 | -0.82880 |
| H | 8.61440 | 2.47250 | 0.00000 |
| H | 11.07560 | 2.47250 | 0.00000 |
| H | 13.53680 | 2.47250 | 0.00000 |
| H | 15.99810 | 2.47250 | 0.00000 |
| H | 18.45930 | 2.47250 | 0.00000 |
| H | 20.92060 | 2.47250 | 0.00000 |
| H | 23.38180 | 2.47250 | 0.00000 |

## Appendix B: Sample Batch Script

Below is a sample SLURM formatted batch script file for use on the University of Central Oklahoma super-computer Buddy. This file is for the GNP + Adenine system.

```
#!/bin/bash
#SBATCH --job-name=g16
#SBATCH --nodes=4
#SBATCH --partition=nodes
#SBATCH --cpus-per-task=20
#SBATCH --output=g16-%j.out

### Of the batch options, it is only recommnded to change "--job-name", "--nodes", and
### "--output". Any other modifications may result in an error.

### It is only recommneded to change the input file in the Gaussian command. If needed
### more g16 options can be added.

#Load Gaussian module
module load Gaussian/g16

#Gaussian scratch directory.
export GAUSS_SCRDIR=/home/$USER/.gaustmp/$SLURM_JOBID
mkdir -p $GAUSS_SCRDIR

#Stop OpenMP from interfering with Gaussian's thread mechanism.
export OMP_NUM_THREADS=1

#Prepare node list for Linda
for n in `scontrol show hostname | sort -u`; do
```

```
  echo ${n}
done | paste -s -d, > snodes.$SLURM_JOBID

#Run Gaussian. It is recommended to only change the input file here. If needed you can
#raise the memory up to 60GB, but doing so may result in an error.
g16 -m=40gb -p=${SLURM_CPUS_PER_TASK} -w=`cat snodes.$SLURM_JOBID` templatepore.com

#Clean up nodes list
rm snodes.$SLURM_JOBID
```

# Appendix C: Sample DOS Mathematica Code

Below is sample code for Mathematica to create the Density of States plot for the GNP + Adenine system. Below that is an image of code to generate plot of two DOS on one graph with Fermi Level.

WOLFRAM MATHEMATICA | STUDENT EDITION  Demonstrations | MathWorld | Wolfram Community

```
data =
 Import[
  "C:\\Users\\nikev\\Desktop\\Graphene Ribbons for Calculation\\Graphene
    Tests\\DOS\\Pore_System\\Adenine\\energiesPoreAdenine.csv"]

erg = 27.2 Flatten[Drop[data, 1]]

Homo = 27.2 * (-0.12977)

Lumo = 27.2 * (-0.12131)


η = 25.0 * 10^-3;

S[x_] := Total[η / (η^2 + (x - erg)^2)];

Plot[S[x], {x, -10, 10}, PlotRange → All, Frame -> True, Axes → False,
 PlotStyle → {Thick, Red}]

Plot[S[x], {x, -6, 0}, PlotRange → All, Frame -> True, Axes → False,
 PlotStyle → {Thick, Red}, GridLines → {{Homo, Lumo}, None},
 GridLinesStyle → Directive[Gray, Dashed]]
```

```
Plot[{SA[x], S3[x]}, {x, -7, -2}, PlotRange → All, PlotStyle → {Red, Blue}, Frame → True, FrameTicks → Automatic,
 FrameTicksStyle → Directive[Bold, 14], Axes → False, PlotLegends → "Expressions", GridLines → {{Ef}, None},
 GridLinesStyle → Directive[Gray, Dashed]]
Plot[{SA[x], S1[x]}, {x, -7, -2}, PlotRange → All, PlotStyle → {Red, DarkGreen}, Frame → True, FrameTicks → Automatic,
 FrameTicksStyle → Directive[Bold, 14], Axes → False, PlotLegends → "Expressions", GridLines → {{Ef}, None},
 GridLinesStyle → Directive[Gray, Dashed]]
```

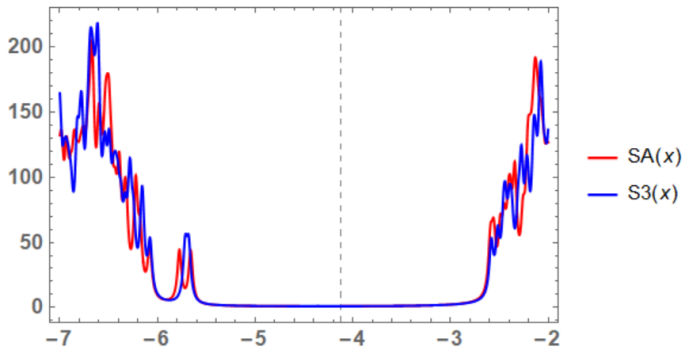

# Appendix D: Scholarly Presentations from this Research

1. **Matthew B. Henry**, Mukesh Tumbapo, and Benjamin O. Tayo, "Physisorption of DNA Bases on Nanoribbons from Graphene, Phosphorene and Silicene," 2020 Virtual Technical Meeting of the Oklahoma Academy of Sciences, November 6, 2020 (Contributor).

2. **Matthew B. Henry** and Benjamin O. Tayo, "Individual Identification of DNA Bases Using Phosphorene Nanomaterials," 2020 National Society of Black Physicists Virtual Meeting, Oral Presentation, November 7, 2020.

3. **Matthew B. Henry** and Benjamin O. Tayo, "DNA Base Detection Using Phosphorene Nanomaterials: First Principle Studies," 2020 Joint Texas APS Virtual meeting, Oral Presentation, November 13, 2020.

4. **Matthew B. Henry** and Benjamin O. Tayo, "DFT Studies of Phosphorene Nanostructures for DNA Sequencing," 2020 American Physical Society Virtual Meeting, Oral Presentation, March 15 - 19, 2021.

5. **Matthew B. Henry**, Mukesh Tumbapo, and Benjamin O. Tayo, "Phosphorene and Silicene Nanodevices for DNA Sequencing: Ab Initio Studies," 2020 American Physical Society Virtual Meeting, Oral Presentation, March 15 - 19, 2021 (Contributor).

# Appendix E: Manuscripts

**Matthew B. Henry**, Mukesh Tumbapo, and Benjamin O. Tayo, "Identification of DNA Bases Using Finite-Size Nanomaterials from Graphene, Phosphorene, and Silicene," (Under Preparation).